

Swc4 protects nucleosome-free rDNA, tDNA and telomere loci to inhibit genome instability

Yue Pan^{a,b}, Can Hu^b, Lin-Jun Hou^b, Yu-Long Chen^b, Jiantao Shi^b, Jia-Cheng Liu^{b,*}, Jin-Qiu Zhou^{a,b,c,*}

^a School of Life Science and Technology, ShanghaiTech University, Shanghai 201210, China

^b The State Key Laboratory of Molecular Biology, CAS Center for Excellence in Molecular Cell Science, Shanghai Institute of Biochemistry and Cell Biology, University of Chinese Academy of Sciences, Chinese Academy of Sciences, Shanghai 200031, China

^c Key Laboratory of Systems Health Science of Zhejiang Province, School of Life Science, Hangzhou Institute for Advanced Study, University of Chinese Academy of Sciences, Hangzhou 310024, China

ARTICLE INFO

Keywords:

Swc4
Nucleosome-free chromatin
DNA recombination
Genome instability

ABSTRACT

In the baker's yeast *Saccharomyces cerevisiae*, NuA4 and SWR1-C, two multisubunit complexes, are involved in histone acetylation and chromatin remodeling, respectively. Eaf1 is the assembly platform subunit of NuA4, Swr1 is the assembly platform and catalytic subunit of SWR1-C, while Swc4, Yaf9, Arp4 and Act1 form a functional module, and is present in both NuA4 and SWR1 complexes. *ACT1* and *ARP4* are essential for cell survival. Deletion of *SWC4*, but not *YAF9*, *EAF1* or *SWR1* results in a severe growth defect, but the underlying mechanism remains largely unknown. Here, we show that *swc4Δ*, but not *yaf9Δ*, *eaf1Δ*, or *swr1Δ* cells display defects in DNA ploidy and chromosome segregation, suggesting that the defects observed in *swc4Δ* cells are independent of NuA4 or SWR1-C integrity. Swc4 is enriched in the nucleosome-free regions (NFRs) of the genome, including characteristic regions of rDNAs, tDNAs and telomeres, independently of Yaf9, Eaf1 or Swr1. In particular, rDNA, tDNA and telomere loci are more unstable and prone to recombination in the *swc4Δ* cells than in wild-type cells. Taken together, we conclude that the chromatin associated Swc4 protects nucleosome-free chromatin of rDNA, tDNA and telomere loci to ensure genome integrity.

1. Introduction

In eukaryotes, the genetic information of DNA is packed into chromatin with a basic unit of nucleosome. A nucleosome consists of a histone octamer (containing two copies of each of the histones H2A, H2B, H3 and H4) wrapped around by ~147 bp of DNA [36,48,58]. The tandem nucleosomes in chromatin are individually flanked by linker DNA sequences, typically 50–60 base-pairs in length [28,63]. In addition to the linker sequences between nucleosomes, thousands of nucleosome-free regions (NFRs) (also referred to as nucleosome-depleted regions, NDRs) are scattered throughout the genome [59,67,69].

In the budding yeast *Saccharomyces cerevisiae* (*S. cerevisiae*), the haploid genome is ~12.5 megabases, but contains approximately $58,000 \pm 1000$ nucleosomes, occupying 81% of the genome [27,43,56]. Accordingly, over 14,000 NFRs, which are typically 80 or more

base-pairs in length, are present throughout the genome [27]. Nucleosome positioning and depletion in the genome are likely determined by a combination of DNA sequence, transcription factors, chromatin modification and ATP-dependent remodeling enzymes, and elongating RNA polymerases [79]. The NFRs can be broadly divided into several categories: (1) the promoter regions of the RNA pol II transcription genes, which are occupied by transcription factors, such as Reb1, Abf1, Rap1 and RSC complex [32,37,46,69]; (2) ARS consensus sequences of replication origins, associated with the pre-replication complex Cdc45-Mcm2-7-GINS [5,74]; (3) transcriptionally active rDNA (ribosomal RNA gene transcribed by RNA pol I/III) arrays, stabilized by TATA-binding protein (TBP), UAF, Rrn3 and Hmo1 [31,60,76,78]; (4) tDNAs (tRNAs genes transcribed by RNA pol III), protected by transcriptional regulators such as Isw1, Isw2 and RSC complex [39,69]; (5) telomeric and subtelomeric regions, bound or regulated by Rap1, Abf1, Reb1 and Tbf1 [18,26,35,54,61,65,69].

* Corresponding authors at: The State Key Laboratory of Molecular Biology, CAS Center for Excellence in Molecular Cell Science, Shanghai Institute of Biochemistry and Cell Biology, University of Chinese Academy of Sciences, Chinese Academy of Sciences, Shanghai 200031, China

E-mail addresses: liujiacheng2015@sibcb.ac.cn (J.-C. Liu), jqzhou@sibcb.ac.cn (J.-Q. Zhou).

NuA4 is an essential histone acetyltransferase complex that is responsible for histone acetylation [2]. It consists of 13 subunits, including Esa1, Eaf1, Swc4 (Eaf2), Eaf3, Yng2 (Eaf4), Eaf5, Eaf6, Eaf7, Epl1, Yaf9, Act1, Arp4 and Tra1 [3,8]. Eaf1 functions as an assembly platform for the formation of the holo-complex [3,53], and Esa1 is the catalytic subunit that possesses acetyltransferase activity [2,13]. A smaller subcomplex called Piccolo NuA4 (containing Esa1, Epl1 and Yng2), catalyzes the global acetylation of histone H4 in a gene-unspecific manner [8,70]. Deletion of *EAF1* disassembles NuA4 complexes, but imposes little effect on cell growth. The SWR1 complex (SWR1-C) is an ATP-dependent histone variant H2A.Z deposition complex. It consists of 14 subunits, including Swr1, Vps72 (Swc2), Swc3, Swc4 (Eaf2), Swc5, Vps71 (Swc6), Swc7, Yaf9, Rvb1, Rvb2, Act1, Arp4, Arp6 and Bdf1 [34,38,55]. Swr1 possesses ATPase activity [55], and plays both the catalytic and the scaffolding functions for the chromatin remodeling activity of SWR1-C [84,85].

Both NuA4 and SWR1-C play important roles in the regulation of gene transcription. NuA4 acetylates the lysine residues on the histone tails of H2A, H2A.Z and H4 at the +1 nucleosomes near promoters [2,30, 52], which in turn enhances the binding of SWR1-C [34,38,55] to the nucleosome-free and the adjacent nucleosomal DNA to substitute H2A for H2A.Z [68,86]. Histone acetylation and H2A.Z deposition at +1 nucleosomes promote gene transcription [4,68]. The functional cross-talk between NuA4 and SWR1-C appears to be mediated by their shared four common subunits Act1, Arp4, Swc4 and Yaf9, which form a submodule to recruit other modules of NuA4 or SWR1-C to chromatin [47,87]. *ACT1* and *ARP4* are essential genes, and deletion of either leads to cell death. Temperature sensitive mutants of *arp4* grown at restrictive temperatures show abnormalities in cell shape, bulk chromatin organization and formation of the chromosome segregation apparatus [19,57]. Biochemical analysis shows that C-terminus of Arp4 binds linker DNA and functions as a DNA-length sensor that regulates nucleosome sliding [10]. *YAF9* is a non-essential gene. The *yaf9Δ* cells grow normally under normal culture conditions, but are hypersensitive to microtubule depolymerizing agents [42]. Yaf9 binds histone H3 through its N-terminus YEATS domain with high preference for acetylated H3K27 [33]. Yaf9 is required for Swc4 association with SWR1-C [84,85].

The role of Swc4 in chromatin integrity is not fully understood [47, 87]. *SWC4*, which encodes a 55 kDa protein, is not essential, but its deletion results in severe slow growth phenotypes [87]. Recent structural analysis of nucleosome-bound NuA4 suggests that the Lys-rich region (including Lys311, Lys314 and Lys316), rather than the N-terminal SANT domain, of Swc4 interacts with the linker DNA of nucleosomes [66]. The C-terminus of Swc4 contains a Yaf9 interacting domain (YID) as it interacts directly with Yaf9 [7]. Truncation of the YID results in defects in H2A.Z deposition, but does not affect cell growth [51,87]. Our previous genetic screen identified Swc4, which is involved in telomere length maintenance [50], but this function of Swc4 is not dependent on the integrity of either NuA4 or SWR1-C [44].

In this study, we further characterized the *swc4Δ* cells at the chromatin level, and found that *SWC4* deletion causes aneuploidy and chromosome segregation errors. Swc4 associates with nucleosome-free regions of the genome, including 5S RNA genes (*RDN5s* in rDNA), tDNAs and telomeres independently of Yaf9, Eaf1 or Swr1. In the absence of Swc4 but not Yaf9, the rDNA, tDNA and telomere loci become more unstable and are highly susceptible to recombination. We propose that Swc4 protects nucleosome-free chromatin of rDNA loci, tDNAs and telomeres to inhibit genome instability.

2. Materials and methods

2.1. Yeast strains and molecular manipulations

The strains used in this study were derived from a BY4743 background and are listed in the Supplementary Table S1. Gene deletion experiments were performed using standard genetic procedures and

PCR-based gene deletion strategies as described previously [45,72]. The epitope tagging strain was constructed using a PCR-based gene modification strategy as described previously [45].

2.2. Growth curve assay

Cells of the indicated genotype were inoculated into 5 ml YPD medium and grown to stationary phase. The cells were then diluted to an OD₆₀₀ of 0.1 in 50 ml of fresh YPD medium. Cell density (OD₆₀₀) was measured hourly. The FACS assay was performed as previously described [25].

2.3. Serial dilution assay

Cells grown to stationary phase in liquid culture were diluted to OD₆₀₀ ~1.0. Fivefold diluted cells were spotted on the indicated plates and incubated for 72 h.

2.4. Chromatin extraction, whole-cell extracts preparation and western blotting

Chromatin was extracted as previously described [62] and whole-cell extracts were prepared by TCA methods. Proteins were separated by SDS-PAGE, and transferred to Immunoblot PVDF membranes (Bio-Rad, cat#1620177). Primary and secondary antibodies diluted with 1 × TBST (50 mM Tris pH 7.5, 150 mM NaCl, 0.05% Tween 20) were incubated overnight at 4 °C and 1 h at room temperature, respectively. The membranes were developed using MiniChemi 610 Plus (Beijing SageCreation Science Company). Antibodies used for western blotting: anti-Myc antibody (Sigma-Aldrich, cat#M4439), anti-Flag antibody (ABclonal, cat#AE005) and anti-H2A antibody (Abcam, cat#188312).

2.5. Cell morphology and fluorescence-activated cell sorting (FACS) assays

Cells were harvested and washed with fresh YPD, followed by sonication. Re-suspended cells in YPD medium were photographed using a Carl Zeiss AxioPlan2 microscope. The FACS assay was performed as previously described [25].

2.6. Immunofluorescence and live cell imaging assays

Immunofluorescence was performed as previously described [88] with a few modifications. Briefly, cells were fixed in 3.7% formaldehyde for 1 h at room temperature, washed twice with 0.1 M potassium phosphate buffer (pH 6.4), and resuspended in sorbitol buffer (1.1 M sorbitol, 0.1 M K₂HPO₄, pH 7.5). Fixed cells were digested for 50 min at 30 °C with 1 µg/ml zymolyase to obtain spheroplasts. Spheroplasts were treated with 1 µg/ml DAPI after antibody incubation. Microscopic preparations were analyzed and imaged at 25 °C using Zeiss LSM880 Ariyscan microscopy (63 ×, oil). Antibodies used for immunofluorescence: anti-β-tubulin antibody (Abmart, cat#M20005M), anti-Nop1 antibody (Santa Cruz, cat#sc-71715), and anti-Myc antibody (Sigma-Aldrich, cat#M4439). Live cells with or without 0.05% MMS treatment were analyzed and imaged at 25 °C using Zeiss LSM880 Ariyscan microscope (63 ×, oil) with YFP filter (514 nm).

2.7. Southern blotting assay

Cells were harvested from liquid cultures. Genomic DNA was extracted by the phenol/chloroform method and digested with *Xba*I (Thermo Scientific). DNA was separated on a 1% agarose gel, and transferred to an Amersham Hybond-N + membrane (GE Healthcare). The telomeric TG₁₋₃ sequence was labeled using DIG-High Prime DNA Labeling and the Detection Starter Kit II (Roche). The probes for

detection of Chr III (*MRC1* and *FEN2*) and Chr XII (*RDN25*) were labeled by High Prime DNA Labeling Kit (Roche) in the presence of [α -³²P]-dCTP, isotope signals were detected by phosphor-image.

2.8. Pulsed field gel electrophoresis (PFGE) assay

Fresh yeast cells were inoculated into 50 ml YPD and incubated at 30 °C until OD₆₀₀ ~1.0. The cells were harvested and washed twice with cold EDTA (50 mM, pH 8.0) buffer, and resuspended in 500 µl CSB buffer (10 mM pH 7.2 Tris-Cl, 20 mM NaCl, 100 mM pH 8.0 EDTA, 4 mg/ml lyticase (Sigma-Aldrich cat#L4025) and 300 µl 2% low melt agarose (Bio-Rad, cat#1613111). 100 µl resuspended cells were added to each plug for 30 min at 4 °C. The solidified agarose plugs were incubated in lyticase buffer (10 mM pH 7.2 Tris-Cl, 100 mM pH 8.0 EDTA, 1 mg/ml lyticase) at 37 °C for 3 h, and then in proteinase K reaction buffer (100 mM pH 8.0 EDTA, 0.2% sodium deoxycholate, 1% sodium lauryl sarcosine) containing 1 mg/ml proteinase K (Sigma-Aldrich, cat#P6556) at 50 °C for 36 h. The plugs were washed 4 times in 25 ml of wash buffer (20 mM Tris, pH 8.0, 50 mM EDTA) for 1 h each time at room temperature with gentle agitation. The plugs were fixed in pulsed field agarose gel (Bio-Rad, cat#1620137) and gel electrophoresis was performed using CHEF-DR II Pulsed Field Electrophoresis System (Bio-Rad). The electrophoresis conditions for the separation of Chr III were as follows: 1% agarose gel; buffer, 0.5 × TBE; temperature, 14 °C; initial switch time, 40 s; final switch time, 80 s; electrophoresis time 18 h; voltage, 6.8 V/cm; angle, 120°. Electrophoresis conditions for the separation of Chr XII: 0.8% agarose gel; buffer, 1 × TAE; temperature, 7 °C; switch time 500 s; electrophoresis time 50 h; voltage, 3 V/cm; angle, 106°. The gel was stained with GelstainRed™ nucleic acid dye (US EVERBRIGHT, cat#S2009L). PFGE gels were imaged using Tanon 2500.

2.9. Chromatin immunoprecipitation sequencing (ChIP-Seq) assay and bioinformatic analysis

ChIP assay was performed as previously described [25] with the following modifications. Immunoprecipitation of cross-linked DNA was probed with monoclonal anti-Myc antibody (Sigma-Aldrich, cat#M4439), anti-Flag antibody (ABclonal, cat#AE005) and anti-Histone H2A (phospho S129) antibody (Abcam, cat#181447). ChIP-qPCR primers were listed in [supplementary Table S8](#). The sequencing library was prepared using the NEBNext Ultra II DNA Library Prep Kit for Illumina (NEB, cat#E7645). Paired-end sequencing reads were trimmed for adapter and low-quality reads using fastp (version: 0.21.0). The trimmed reads were then aligned to the reference genome (Saccharomyces genome database: <https://www.yeastgenome.org>) using the subcommand mem of BWA (version: 0.7.15-r1140) with default parameters. The Bam file was sorted and de-duplicated using the samtools (version: 1.4). MACS2 (Version: 2.1.1.20160309) was used to call Swc4 ChIP-seq peaks with the q value < 0.05. The gene transfer format (GTF) file for *S. cerevisiae* was used to annotate the ChIP-seq peaks. To obtain the Swc4 signals in the single copy of the rDNA repeat (~9.1 kb), the reads were aligned to the reference sequence (rDNA reference) extracted from *S. cerevisiae* (sacCer3), Chr XII: 451, 418–460,554 bp. The rDNA reference was used in [Fig. 3D](#) and [Fig S7D](#).

2.10. Assay for Targeting Accessible-Chromatin with high-throughput sequencing (ATAC-seq)

5 × 10⁴ spheroplasts were centrifuged at 2000 g for 5 min and washed once with sorbitol buffer. Cell pellets were resuspended in 50 µl of Tn5 digestion mix using the TruePrep DNA Library Prep Kit V2 (Vazyme#TD501-01). VAHTS DNA Clean Beads (Vazyme#N411) were used to purify the Tn5 digested products. The DNA library was amplified by PCR using the TruePrep Index Kit V2 (Vazyme#TD202) for Illumina sequencing. PCR products were purified by using VAHTS DNA Clean Beads (Vazyme#N411) and eluted in 20 µl distilled H₂O.

Raw read files were first processed using Trim Galore version 0.5.0 (Babraham Institute) to trim low-quality reads and remove adapters. Bowtie2 version 2.3.1 was used to map reads to *S. cerevisiae* using the parameter ‘-t -q -N 1 -L 25 -X 2000 –no-mixed –no-discordant’, where ‘-X 2000’ allows the maximum fragment length to be 2000 bp, ‘–no-mixed’ suppresses unpaired alignments for paired reads and ‘–no-discordant’ suppresses discordant alignments for paired reads. To minimize PCR and sequencing optical bias, the Picard version 2.18.7 subcommand Mark-Duplicates was used to remove duplicates (defined as the same start and end positions) and CollectInsertSizeMetrics was used to estimate fragment size distribution. Samtools version 1.4 was used manipulate the SAM file. Specifically, the view subcommand with the ‘-q 10 -b’ parameter was used to remove low-quality, unmapped, unpaired and duplicated reads, as well as convert to BAM format. Subcommands sort and index with default parameters were used to sort and index BAM files. BigWig format files were generated via bamCoverage version 1.5.11 with the parameter ‘-bs 10 –normalizeUsingRPKM’. HMMRATAC version 1.2.10 was used to call peaks using the sorted BAM file. The gene transfer format (GTF) file for *S. cerevisiae* was used to annotate the ATAC-seq reads.

2.11. Recombination assay

The recombination assay was performed as previously described [64] with a few modifications. Briefly, to detect recombination between two *SUP53* tRNA^{Leu} genes, we constructed a *SUP53* tRNA^{Leu}-*URA3-SUP53* tRNA^{Leu} sequence (SUS sequence). The sequence of the first copy of tRNA^{Leu}, adjacent to the *LEU2* promoter, was fused to the coding sequence of a *URA3* gene. The 200 bp sequence downstream of the *LEU2* gene was fused to the 3' end of *URA3*. A second copy of the *SUP53* gene was fused to the 200 bp downstream of the 3' end of the *URA3* gene, in the same direction as the first *SUP53* tRNA^{Leu} sequence. The SUS sequence was then inserted into Chr III of strain *swc4Δ* or *yaf9Δ* of the BY4743 background. The wild-type (WT^{SUS}), and single deletion mutants (*swc4Δ*^{SUS} and *yaf9Δ*^{SUS}) were obtained by tetrad dissection after sporulation.

Three independent clones from a single spore were used in the marker-loss experiments. Individual colonies were cultured in Ura-media to ensure the retention of the *URA3* genes. Cells were harvested and resuspended in sterile water. Cells were adjusted to the appropriate concentration and transferred to the Ura⁺ and 5'-FOA plates, respectively. Cells were plated on 5'-FOA medium to select for clones that had undergone homologous recombination between two identical *SUP53* tRNA^{Leu} genes. Rate of 5'-FOA resistance = number of clones on the 5'-FOA plate/ number of clones on the Ura- plate.

3. Results

3.1. Deletion of *SWC4* causes aneuploidy, chromosome segregation errors, and chromosome rearrangement independently of *NuA4* or *SWR1-C*

In the previous *S. cerevisiae* genome deletion project, *SWC4* was classified as an essential gene [20], probably because its deletion causes severe slow growth [87]. Given that Swc4 is a common subunit of NuA4 and SWR1-C, it remains possible that the slow growth of *swc4Δ* cells is due to synthetic defects of NuA4 and SWR1-C. To test this, we constructed diploid strains that are heterozygous for *SWC4*, and the single deletion mutants (*swc4Δ*) were obtained by tetrad dissection after sporulation. We examined the growth of the *swc4Δ*, *yaf9Δ*, *eaf1Δ* and *swr1Δ* cells. The results showed that in both liquid and solid media, the *swc4Δ* cells had a much slower growth rate than the wild-type cells, whereas *yaf9Δ*, *eaf1Δ* or *swr1Δ* cells had a comparable growth rate to the wild-type cells ([Fig. 1A](#), left panel and [Fig S1A](#)). These results suggest that the role of Swc4 in promoting cell growth is independent of the integrity of either NuA4 or SWR1-C.

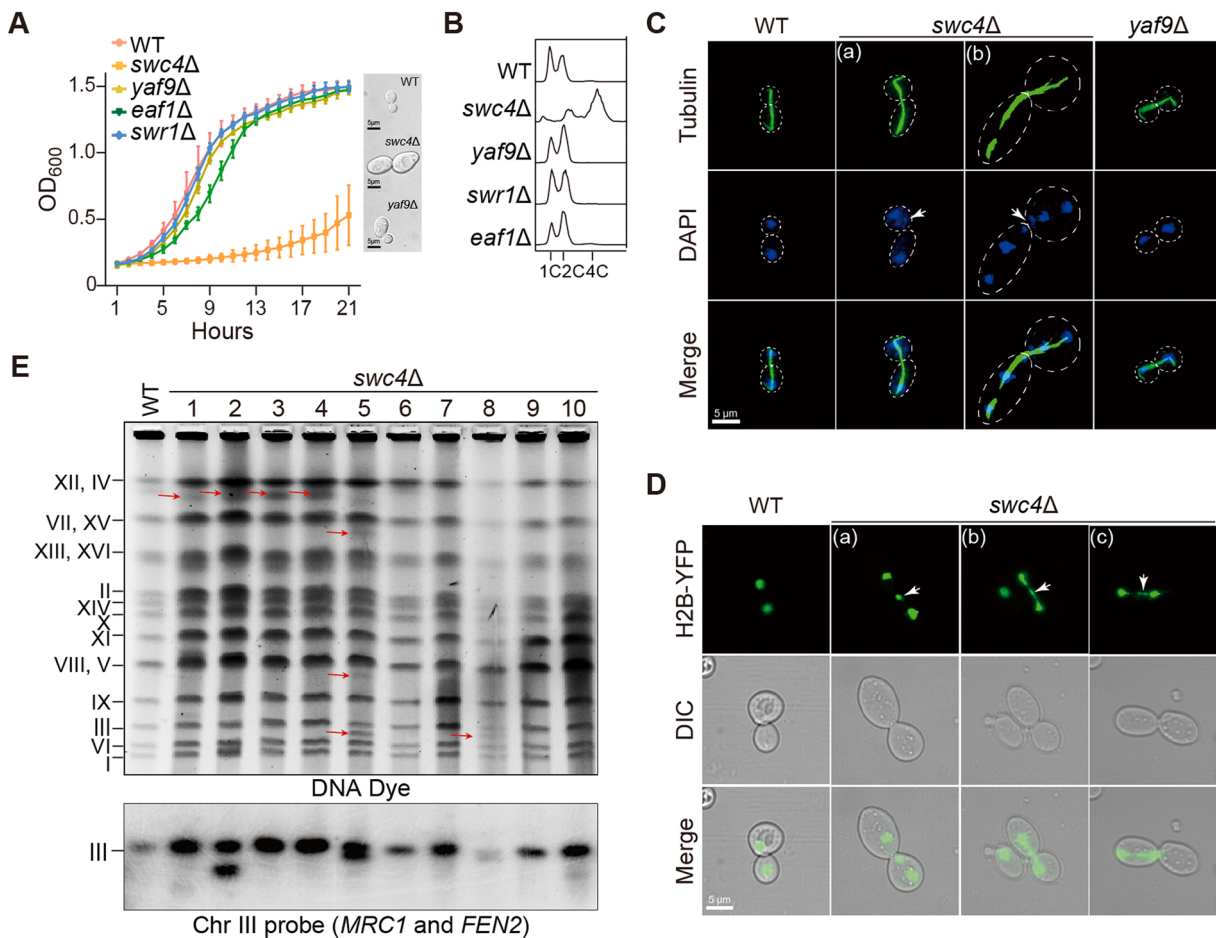


Fig. 1. Characterization and chromosome breakage detection in *swc4Δ* cells. (A) Growth curves of the indicated strains. Error bars represent standard deviation (s.d), $n = 3$. Right pictures are the representatives of the cell morphologies of wild-type, *swc4Δ* and *yaf9Δ* cells. (B) FACS analysis of DNA content in wild-type, *swc4Δ*, *yaf9Δ*, *swr1Δ* and *eaf1Δ* cells. The cells of the indicated genotypes grown to mid-log phase were analyzed by FACS. (C) Immunofluorescence of tubulin and nucleus in wild-type, *swc4Δ* and *yaf9Δ* cells. Anti-tubulin antibody and DAPI were used to detect microtubule and nucleus, respectively. The aberrant chromosome segregation events are indicated by white arrows. The cell shape is depicted by dotted line. (D) Live cell imaging of chromosomes. Wild-type and *swc4Δ* strains harboring YFP-tagged H2B were imaged by Zeiss LSM880 Ariyscan microscopy ($63 \times$, oil). The aberrant chromosome segregation events in the representative cells are indicated by white arrows. (E) The upper panel, karyotype analysis of wild-type and *swc4Δ* strains by pulsed field gel electrophoresis (PFGE). The chromosome number is indicated on the left of the panel, and the aberrant chromosomes are indicated by red arrows. The lower panel, Southern blotting analysis of the Chr III in wild-type and *swc4Δ* strains. The ORFs of the genes *MRC1* and *FEN2* (located on the left and the right arms of Chr III, respectively) were labeled to probe Chr III.

To gain the insight into the slow growth of *swc4Δ* cells, we examined the morphologies of the *swc4Δ* and the *yaf9Δ* cells. The *swc4Δ* cells were much larger in cell size than the wild-type and the *yaf9Δ* cells (Fig. 1A, right panel). Quantitatively, the *swc4Δ* strain had ~43% dumbbell-shaped cells and ~23% abnormal cells (three or four cells connected together), which were significantly higher than those in the wild-type and the *yaf9Δ* strains (Fig S1B). A CEN-plasmid carrying the *SWC4* gene could complement the slow growth of *swc4Δ* cells (Fig S1C). FACS analysis was also performed to determine the DNA content of the isogenic strains: the *yaf9Δ*, *swr1Δ* and *eaf1Δ* cells had normal 1C and 2C as the wild-type cells (Fig. 1B). In contrast, most of the *swc4Δ* cells had either 2C or 4C, few of the *swc4Δ* cells contained 1C, and a small fraction of *swc4Δ* cells had less than 1C (Fig. 1B). These results suggest that deletion of *SWC4*, but not *YAF9*, *SWR1* or *EAF1*, causes aneuploidy. We attempted to use alpha-factor to arrest the *swc4Δ* (*MATα* type) cells at G1 phase, and use wild-type (*MATα* type) cells as a positive control. The results showed that wild-type and *swc4Δ* cells were able to respond to alpha-factor and arrested in G1, but a large number of *swc4Δ* cells had undergone endoreduplication of the genome, and become homozygous diploid a/a cells (Fig S1D).

To detect chromosomal ploidy in the *swc4Δ* cells, we examined mitotic spindle pole bodies and nuclear DNA by immunofluorescence for

tubulin and DAPI staining, respectively. The bipolar separation of spindle pole bodies (tubulin immunofluorescence), associated with nucleus DNA (DAPI staining), was normal in the *swc4Δ*, *yaf9Δ* and the wild-type cells (Fig. 1C). Nuclear DNA segregated normally in wild-type and *yaf9Δ* cells (Fig. 1C). In contrast, the nuclear DNA in some of the *swc4Δ* cells appeared to be fragmented (Fig. 1C, *swc4Δ* (a)). Some of *swc4Δ* cells with bi-nuclei failed to divide: one progeny contained two DAPI signals (nuclei) of almost equal density, the other contained a few uneven DAPI signals (Fig. 1C, *swc4Δ* (b)), suggesting that the deletion of *SWC4* but not *YAF9* results in chromosome segregation defects. To further assess the chromosome segregation defects in the *swc4Δ* cells, we visualized chromosomes by detecting YFP-tagged H2B in living cells. Consistently, a large proportion of the *swc4Δ* cells exhibited chromosome segregation defects that were rare in wild-type cells (Fig. 1D). For example, (1) chromosome breakage occurred in the representative cell shown in *swc4Δ*-a of Fig. 1D; (2) chromosome bridging was detected in *swc4Δ*-b of Fig. 1D; (3) chromosomes remained in one cell instead of two in *swc4Δ*-c of Fig. 1D. Notably, three or four interconnected cells were frequently observed in the H2B-YFP *swc4Δ* strain (Fig S2A). These results further indicated that *Swc4* is required for proper chromosome segregation. A CEN-plasmid carrying the *SWC4* gene was able to rescue the chromosome segregation defect caused by *SWC4* deletion (Fig S2B).

To investigate the abnormal chromosome segregation at the molecular level, we used pulsed field gel electrophoresis (PFGE) to examine the karyotype of the *swc4Δ* and *yaf9Δ* cells. The 16 chromosomes in the wild-type cells were separated as previously reported (Fig. 1E, upper panel) [71]. Some of the chromosomes migrated to the same position in the gel because they were too close in size to be distinguishable under the experimental conditions (Fig. 1E, upper panel) [71]. Interestingly, at least 6 of the 10 independent *swc4Δ* clones contained chromosomal bands that were not found in wild-type cells (Fig. 1E, indicated by red arrows and Fig S3A). We performed a Southern blot assay using the probes for the *MRC1* and *FEN2* genes in Chr III, and found that out of 10 clones, the clones 2, 5, 8 and 10 contained “broken and/or rearranged” Chr III (Fig. 1E, lower panel), confirming that deletion of *SWC4* results in chromosomal rearrangement. The chromosomes of the *yaf9Δ* cells showed the same migration patterns as those of the wild-type cells (Fig. S3A). We transferred a CEN-plasmid containing the *SWC4* gene into clones 1, 4, 5, 8 and 10, and examined their karyotypes by PFGE. The rearranged chromosomes in clones 4, 5, 8 and 10 were not changed after reintroduction of the wild-type *SWC4* gene (Fig S3C), further suggesting that *Swc4* is required for genome stability.

3.2. Chromosome instability in *swc4Δ* cells activates the spindle assembly checkpoint, but not the Rad53- and Chk1-mediated DNA damage checkpoint

Chromosome breakage represents a catastrophic consequence of double-stranded DNA breaks (DSBs) that usually activates the cell cycle checkpoint, leading to cell cycle arrest and cell death if DSBs are not repaired. Consistent with this, over 90% of *swc4Δ* pRS316-*SWC4* cells die upon loss of the wild-type copy of *SWC4* [44]. The DNA damage and replication checkpoint is initiated by the phosphatidylinositol 3' kinase (PI3K)-related kinases (PIKKs) Mec1 and Tel1, which phosphorylate

Rad9. Phosphorylations of the downstream effectors Rad53 and Chk1 results in cell cycle arrest at G1/S, S and G2/M phases (Fig. 2A) [16,40]. For the G2/M to anaphase, the spindle assembly checkpoint (involving Bub1, Mad1/Mad2/Mad3) prevents APC-Cdc20 complex formation and anaphase entry (Fig. 2A) [75]. We examined the phosphorylation of Rad53 (Fig. 2B) or 13Myc-tagged Chk1 (Fig. 2C) in *swc4Δ* cells. As negative and positive controls, untreated and MMS (methyl methanesulfonate, a genotoxin) treated wild-type cells showed low and robust Rad53 or Chk1 phosphorylation, respectively (Fig. 2B and C). Notably, *swc4Δ* cells showed as little phosphorylated -Rad53 or -Chk1 as wild-type cells (Fig. 2B and C). Upon MMS treatment, Rad53 or Chk1 phosphorylation occurred efficiently in *swc4Δ* cells (Fig. 2B and C), indicating that deletion of *SWC4* did not disrupt the Rad53 or Chk1 checkpoint pathways. Accordingly, deletion of either *RAD9* or *CHK1* could hardly rescue the slow growth phenotype of *swc4Δ* cells (Fig S4A). These results suggest that *SWC4* deletion does not activate Rad53- and Chk1-associated DNA damage checkpoints.

We next examined the phosphorylation of the 3Flag-tagged Mad1 in *swc4Δ* cells. The nocodazole treated wild-type cells showed significant Mad1 phosphorylation (Fig. 2D, positive control) [24]. Interestingly, *swc4Δ* cells displayed higher levels of phosphorylated-Mad1 than wild-type cells (Fig. 2D), suggesting that *SWC4* deletion activates the spindle assembly checkpoint. Accordingly, deletion of *MAD1* could modestly alleviate the slow growth defect of *swc4Δ* cells (Fig. 2E), supporting the notion that the defects of chromosome segregation in *swc4Δ* cells activate the spindle assembly checkpoint. We attempted to construct *swc4Δ bud1Δ* and *swc4Δ mad2Δ* double deletion strains, but they were not viable (Fig S4B and C).

At the chromatin level, phosphorylation of histone H2A at serine 129, termed γ-H2A (γ-H2AX in mammals), is an early event occurring at DSB sites [14]. We measured γ-H2A levels in wild-type, *swc4Δ*, *yaf9Δ*, *swr1Δ* and *eaf1Δ* cells by Western blotting. Consistent with the previous

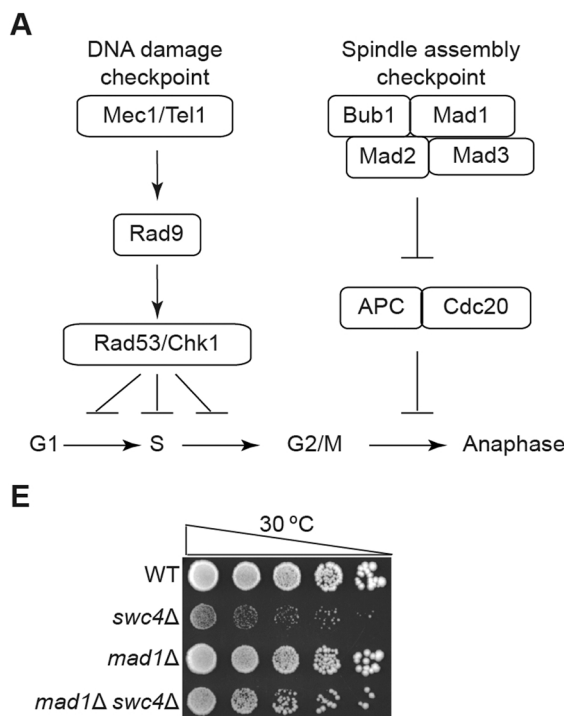


Fig. 2. Checkpoint activation analyses in *swc4Δ* cells. (A) The schematic diagram of the DNA damage and spindle assembly checkpoints. (B and C) Western blotting analysis of Rad53 and Chk1 phosphorylation. Whole cell proteins of wild-type and *swc4Δ* cells were extracted, the Rad53 and Chk1 phosphorylations were monitored by anti-Rad53 antibody and anti-Myc antibody, respectively. “+”, cells were treated with 0.05% MMS for 2 h, “-”, cells were untreated with 0.05% MMS. (D) Western blotting analysis of Mad1 phosphorylation monitored by anti-Flag antibody. 10 µg/ml nocodazole-treated 4 h (noc) and untagged (no-tag) wild-type cells were used as positive and negative controls, respectively. (E) Cell growth analysis. Five-fold serial dilutions of the isogenic strains (labeled on left) were spotted onto YPD plate and grown for ~72 h at 30 °C. (F) Western blotting analysis of the γ-H2A (phosphorylation of H2A serine 129) level. Whole-cell proteins of indicated strains were extracted, the γ-H2A and H2B (loading control) were monitored by anti-γ-H2A antibody and anti-H2B antibody, respectively.

studies [14,80], γ -H2A was detectable in wild-type cells, and MMS (methyl methanesulfonate) treatment dramatically increased γ -H2A levels (Fig. 2 F). Notably, deletion of *SWC4* significantly increased the γ -H2A level, much higher than that in the wild-type, *yaf9 Δ* , *swr1 Δ* and *eaf1 Δ* cells (Fig. 2 F). Furthermore introducing either the *hta1-S129A* or *hta1-S129E* mutation, which abolishes phosphorylation of H2A-S129 by Mec1 and/or Tel1 [14], into *swc4 Δ* cells further exacerbated the slow growth (Fig S4D), suggesting that γ -H2A is critical for DSB repair upon loss of *Swc4*. These results further suggest that the observed chromosome breakage results from the dysfunction of *Swc4*, but not from the loss of the integrity of either NuA4 or SWR1-C.

3.3. *Swc4* associates with *RDN5s*, tDNAs and telomeres independently of *Yaf9*, *Eaf1* or *Swr1*

Swc4 forms a subcomplex with *Yaf9*, *Arp4* and *Act1* to recruit other modules of NuA4 or SWR1-C to chromatin [47], and *Swc4* and *Arp4* have been reported to interact with DNA [10,66]. To investigate whether the association of *Swc4* with chromatin requires *Yaf9*, we extracted the chromatin and detected chromatin-associated *Swc4* in the wild-type and the *yaf9 Δ* cells. Western blotting results showed that *Swc4* was co-fractionated with chromatin in both cells (Fig. 3A), indicating that the absence of *Yaf9* does not affect the association of *Swc4* with chromatin.

We then performed ChIP-seq assays in the wild-type, *yaf9 Δ* , *eaf1 Δ* and *swr1 Δ* cells. The 13Myc-tagged *Swc4* was precipitated, and the genomic DNA cross-linked to 13Myc-tagged *Swc4* was sequenced and analyzed (see Material and Methods). The ChIP-seq signals from *Swc4* were scattered across all of the 16 chromosomes (Fig S5), and were not attenuated when *YAF9*, *EAF1* or *SWR1* was deleted (Fig S5). In each

strain examined, the ChIP-seq peaks from two replicates were reproducible (with an average of 60% common peaks) (Fig S6A). The peaks identified in the *yaf9 Δ* , *eaf1 Δ* or *swr1 Δ* cells overlapped strongly with those in wild-type cells (Fig S6B). These results were consistent with *Swc4* associating with chromatin independently of *Yaf9*, *Eaf1* or *Swr1*.

Region-set enrichment analysis of the ChIP-seq data revealed that *Swc4* was preferentially associated with the genomic loci of rDNA, tDNA, telomere/subtelomeric X- and Y'-element, and ARS (feature regions, Fig. 3B, left panel and Supplementary Table S2), which are representative of NFRs [26,5,69]. *Swc4* was also associated with the sequences encoding some of the snoRNAs, ncRNAs and introns (feature regions, Fig. 3B, left panel). The apexes of these ChIP-seq signals were mapped to the nucleosome depleted regions rather than to the nucleosome-occupied sequences encoding snoRNAs, ncRNAs and introns themselves (Supplementary Tables S3-S6, ChIP-seq peak files). These data suggest that *Swc4* preferentially binds to the NFRs in the yeast genome. Interestingly, in the absence of *Yaf9*, *Eaf1* or *Swr1*, *Swc4* appeared to associate with many more genomic loci, which were also clustered in rDNA, tDNA and telomere regions (Fig. 3B, right panel and Fig S7A-7B). One explanation is that loss of *YAF9*, *EAF1* or *SWR1* leads to the collapse of NuA4 or SWR1-C, and more *Swc4* proteins are translocated to the NFRs. The other explanation is that deletion of *YAF9*, *EAF1* or *SWR1* increases the local residence time of *Swc4* at the NFRs. Taken together, these data indicate that *Swc4* associates with NFRs at rDNA, tDNAs and telomeres, and that the association of *Swc4* with NFRs is negatively regulated by the other submodules of NuA4 or SWR1-C.

The rDNA loci on the right arm of Chr XII contain 100–150 tandem repeats of rRNA genes [29,73,83]. The extremely prominent ChIP-seq reads were aligned to rDNA loci, and were approximately 100-fold higher than those at other loci in Chr XII (Fig. 3C and Fig S7C) likely

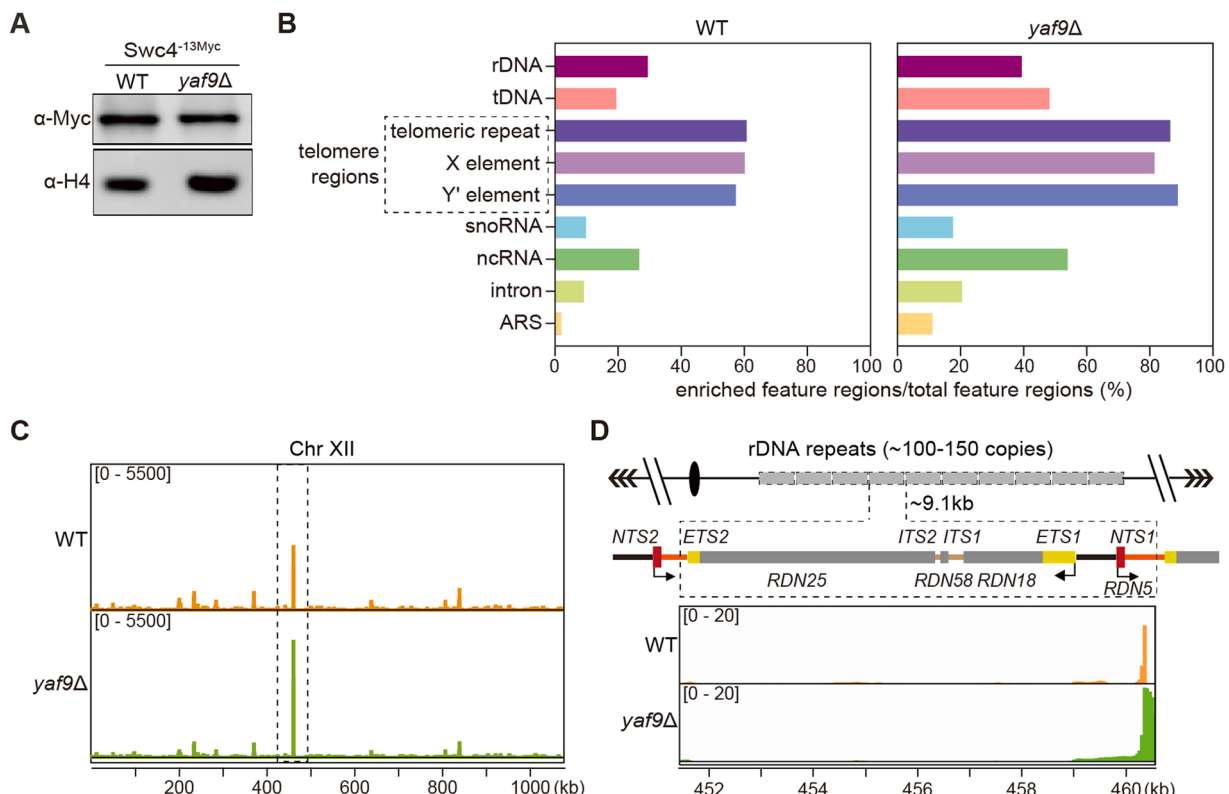


Fig. 3. ChIP-seq analysis of chromatin association of *Swc4* in wild-type and *yaf9 Δ* cells. (A) Western blotting analysis of chromatin associated *Swc4*. Chromatin from the indicated strains (labeled on top) was extracted, and 13Myc-tagged *Swc4* and histone H4 were detected with anti-Myc antibody and anti-H4 antibody (loading control), respectively. (B) *Swc4*-enriched feature regions in the genome. X-axis: the percentage of *Swc4*-enriched region in the total feature region. (C) IGV browser shot comparison of ChIP-seq peaks at Chr XII in wild-type and *yaf9 Δ* cells. (D) IGV browser shot comparison of ChIP-seq peaks at single copy of rDNA repeat. The schematic of rRNA genes in one rDNA repeat and their transcription directions are shown at the top. The log₂ (13Myc-tagged *Swc4* treat/no-tag control) enrichments were shown.

due to the high copy number of rRNA genes. Each ~9.1 kb repeat of an rRNA gene contains one copy of *RDN37* (encoding 18S/5.8S/28S rRNAs), one copy of *RDN5* (encoding 5S rRNAs), two internal transcribed spacers (*ITS1* and *ITS2*), two external transcribed spacers (*ETS1* and *ETS2*) and two non-transcribed spacers (*NTS1* and *NTS2*) (Fig. 3D, top schematic of rRNA genes) [83]. We analyzed the signal distribution

of Swc4 in the specific rRNA genes, and found that Swc4 bound the *NTS1*, which is immediately downstream of the *RDN5*, but not other rRNA genes (Fig. 3D and Fig S7D).

We also performed a detailed analysis of Swc4 accumulation at all of the tDNA and telomere regions, and the heatmap results showed that Swc4 was enriched at large parts of both tDNA and telomere regions in

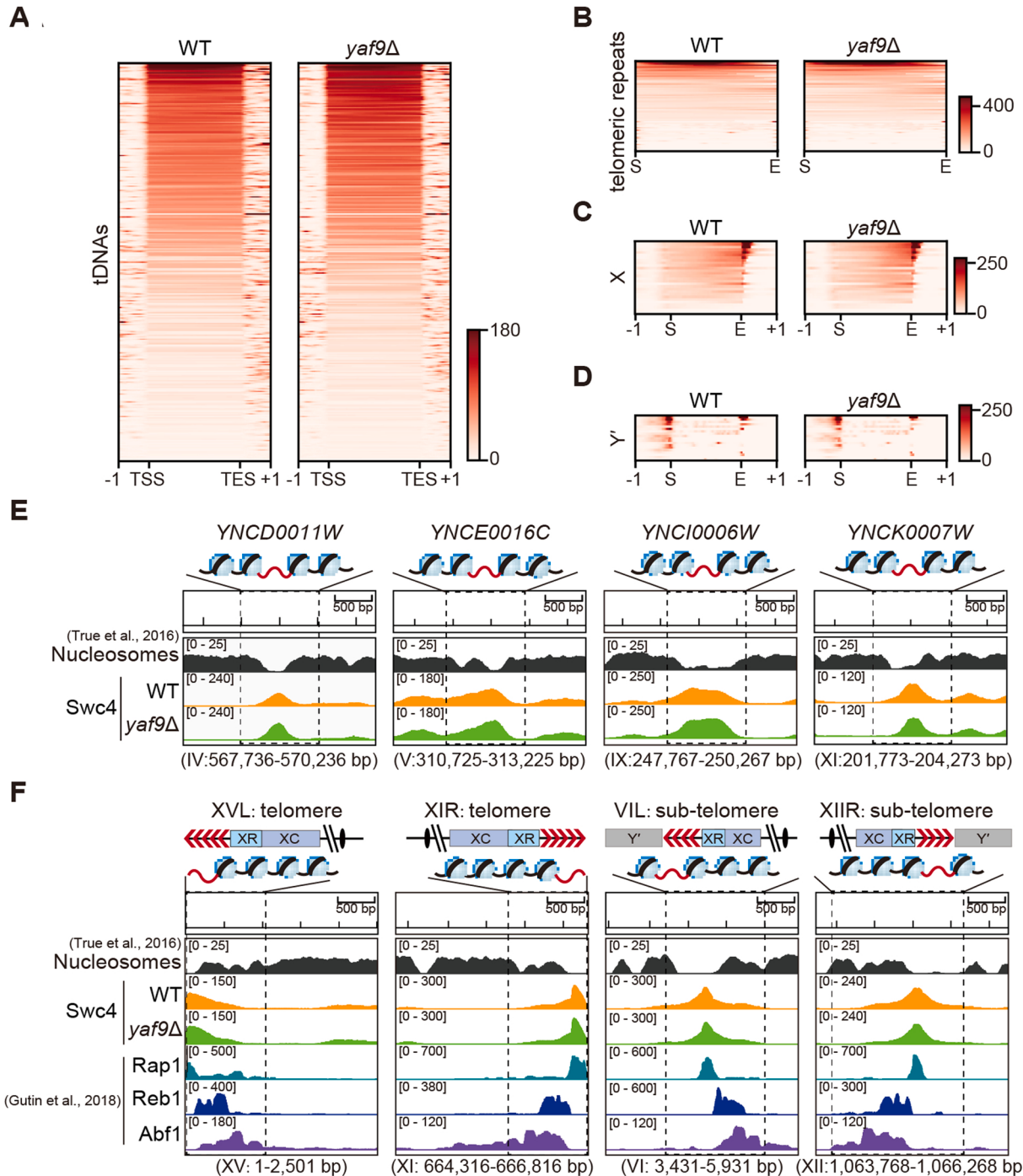


Fig. 4. Swc4 associates with chromatin at tDNA and telomere regions independently of Yaf9. (A-D) Heatmaps of the enrichment of Swc4 at all tDNA (A) and telomere (B-D) regions in wild-type and *yaf9Δ* cells. (A) “TSS”, transcription start site. “TES”, transcription ending site. “-1” and “+1”, 1 kb upstream and downstream of “TSS” and “TES”, respectively. (B-D) “S”, the first base of 5’ subtelomeric X- or Y'-elements. “E”, the last base of 3’ subtelomeric X- and Y'-elements. “-1” and “+1”, 1 kb upstream and downstream of “S” and “E”, respectively. (E) IGV browser shots comparison of nucleosomes [81] and 13Myc-tagged Swc4 in four specific tDNA regions. The schematic diagrams of tDNA regions are shown at the top: the red line, gene body of tDNA; light blue oval wrapped by black curve, nucleosomes adjacent to the tDNA. (F) IGV browser shots comparison of nucleosomes, 13Myc-tagged Swc4 and TF (Reb1, Abf1 and Rap1) signals [22] in four specific telomere regions. The schematic diagrams of telomere and subtelomeric X- and Y'-elements are shown at the top: red arrow and lines, TG repeats; XR and XC, subtelomeric X elements; Y', subtelomeric Y' elements. The schematic diagrams have not been scaled. The numbers at the bottom: genome sequence information from *S. cerevisiae*/sacCer3.

wild-type, *yaf9Δ*, *eaf1Δ* and *swr1Δ* cells (Fig. 4A–D and Fig S8A–D). At tDNAs, Swc4 appeared to be significantly enriched in gene bodies (Fig. 4A and Fig S8A). For example, at four tRNA gene loci (YNCD0011W, YNCE0016C, YNCI0006W and YNCK0007W), Swc4 and nucleosome occupancy were mutually exclusive (Fig. 4E). The association of Swc4 with tDNAs was not affected by the deletion of *YAF9*, *EAF1* or *SWR1* (Fig. 4E and Fig S8E).

Swc4 enrichment was observed at most of the telomere regions (Fig. 4B–D and Fig S8B–D). Notably, the Swc4-associated DNA contained telomeric TG_{1–3}/C_{1–3}A sequences, which were either at the end of a telomere or between X- and Y'- elements (Fig. 4B–D and Fig S8B–D). For example, Swc4 occupied the telomeric regions of Chr XV left arm (Tel XVL) and Chr XI right arm (Tel XIR), and subtelomeric regions of Chr VI left arm (Tel VIL) and Chr XII right arm (Tel XIIR) (Fig. 4F, schematic graphs on top). Compared with the previously published data for histone H3 (nucleosome signals) [81], Reb1, Abf1 and Rap1 [22], Swc4 was enriched at loci without nucleosome signals, and overlapped with the Rap1 sites, but not with Abf1 and Reb1 nucleosome-containing sites (Fig. 4F). Furthermore, the enrichment of Swc4 with telomere regions in the *yaf9Δ*, *eaf1Δ* and *swr1Δ* cells showed a similar pattern to that in the wild-type cells (Fig. 4F and Fig S8F), indicating that the association of Swc4 with telomere regions is also independent of *Yaf9*, *Eaf1* and *Swr1*.

Previous studies have shown that both NuA4 and SWR1-C (including the Swc4-Yaf9-Arp4-Act1 submodule) target many +1 nucleosomes of gene transcription start sites (TSSs) in the yeast genome [68,86]. We analyzed the enrichment of Swc4 in the 6293 TSSs (not including tDNAs) of the whole genome, and found that only in a small fraction of TSSs, Swc4 was enriched at +1 and/or –1 nucleosome regions (Fig S9) [68,86]. In the *yaf9Δ*, *eaf1Δ* and *swr1Δ* cells, the overall enrichments of Swc4 around TSSs were slightly decreased (Fig S9). We speculated that the decrease of Swc4 at TSSs (Fig S9) resulted in the slight increase of Swc4 at nucleosome-free rDNA, tDNA and telomere loci in the *yaf9Δ*,

eaf1Δ and *swr1Δ* cells (Fig. 3B, Fig S7A and S7B).

3.4. *SWC4* deletion increases the chromatin accessibility of *RDN5s*, tDNAs and telomeres

The “open chromatin” of nucleosome-free rDNA, tDNA and telomere loci are the most fragile sites in the genome [11,80,9]. We hypothesized that the association of Swc4 with the nucleosome-free rDNA, tDNA and telomere loci plays a protective role. In the absence of Swc4, the “open chromatin” of nucleosome-free rDNA, tDNA and telomere loci becomes more susceptible and vulnerable to nuclease attack, leading to a further increase in chromatin accessibility. Therefore, we performed ATAC-seq assays and analyzed the number, width (number of bases) and height (counts) of ATAC-seq peaks to assess the chromatin accessibility [1]. The ATAC-seq peaks were identified using the software HMMRATAC version 1.2.10 (see Materials and Methods). A total of 964 peaks were detected in wild-type cells, (Fig. 5A), including NFRs such as *RDN5s*, tDNAs and telomeres (Fig. 5B, left panel and Supplementary Table S7). In *swc4Δ* cells, there were 2598 peaks (Fig. 5A), of which 897 peaks were shared between wild-type and *swc4Δ* cells, and 1701 peaks were specific to the *swc4Δ* cells (Fig. 5A), indicating that the absence of Swc4 significantly increased the chromatin accessibility. Statistical analysis revealed that the width of the overlapping 897 peaks was significantly expanded in the *swc4Δ* cells compared to the wild-type cells (Fig. 5C). Consistently, *RDN5-1* and *RDN5-2* became more accessible to the Tn5 transposase in the absence of Swc4 (Fig. 5D). Notably, 75 ATAC-seq signals for tDNAs (~300 in total) were detected in both the wild-type cells and the *swc4Δ* cells, and an additional 158 ATAC-seq signals for tDNAs were specifically detected in the *swc4Δ* cells (Fig. 5B and Supplementary Table S7), indicating increased accessibility of tDNAs. For telomere regions (including 31 telomeres, 28 subtelomeric X elements and 19 subtelomeric Y' elements in Supplementary Table S7), 59 ATAC-seq signals were detected in the wild-type cells and the *swc4Δ* cells, and an

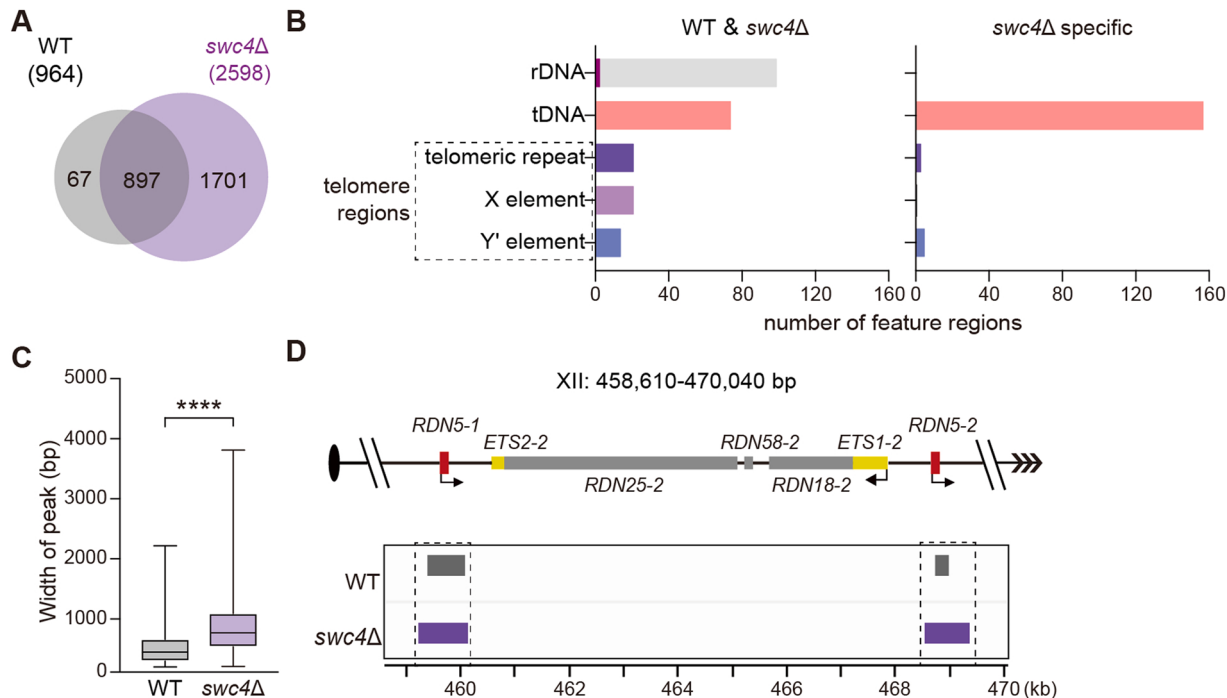


Fig. 5. ATAC-seq analysis of chromatin in wild-type and *swc4Δ* cells. (A) Venn diagram showing the ATAC-seq specific and overlapped peaks in wild-type and *swc4Δ* cells. Peaks were called using HMMRATAC software (version 1.2.10). (B) Distribution of the peaks in different feature regions of the yeast genome. For rDNA, purple column, different rRNA genes occupied by ATAC-seq peaks; gray columns, theoretical calculation of ~100 copies *RND5-1* on yeast genome. (C) The width of the 897 shared peaks in wild-type and *swc4Δ* cells. ****, P < 0.0001 (Student's t-test). (D) Genome browser shots showing the width of the ATAC-seq peaks at *RND5-1* and *RND5-2* in rDNA loci in wild-type and *swc4Δ* cells. The schematic of *RND5-1* and *RND5-2* are shown at the top: genome sequence information from *S. cerevisiae*/sacCer3. The width files of wild-type and *swc4Δ* cells were annotated with the software HMMRATAC version (1.2.10).

additional 11 signals were specifically detected in the *swc4Δ* cells (Fig. 5B and Supplementary Table S7). Taken together, these data indicate that *SWC4* deletion increases the accessibility of open chromatin, particularly at rDNA, tDNA and telomere loci.

The heatmap results showed that in *swc4Δ* cells, the ATAC-seq counts in tDNA and telomere regions were higher than those in wild-type cells (Fig. 6A-D). At four tDNAs (YNCD0011W, YNCE0016C, YNCI0006W and YNCK0007W) and four specific telomeric/subtelomeric regions (i.e. the telomeric regions of Tel XVL and Tel XIR), the height and width of the peaks in the *swc4Δ* cells were higher and wider, respectively, than those in the wild-type cells (Figs. 6E and 6F). These results supported the

hypothesis that Swc4 protects the NFRs of RDN5s, tDNAs and telomeres.

3.5. Genome instability is increased at rDNA loci in the *swc4Δ* cells

The rDNA loci, tDNAs and telomeres are representative of fragile sites in the yeast genome that are prone to damage [49,80]. We investigated whether the loss of *SWC4* exacerbates genomic instability at these vulnerable sites. To examine the stability of rDNA loci, we performed PFGE analysis followed by Southern blotting with an rDNA probe. The size of Chr XII remained unchanged in both the wild-type and the *yaf9Δ* cells (Fig. 7A and Fig. S3B). In contrast, in different clones of

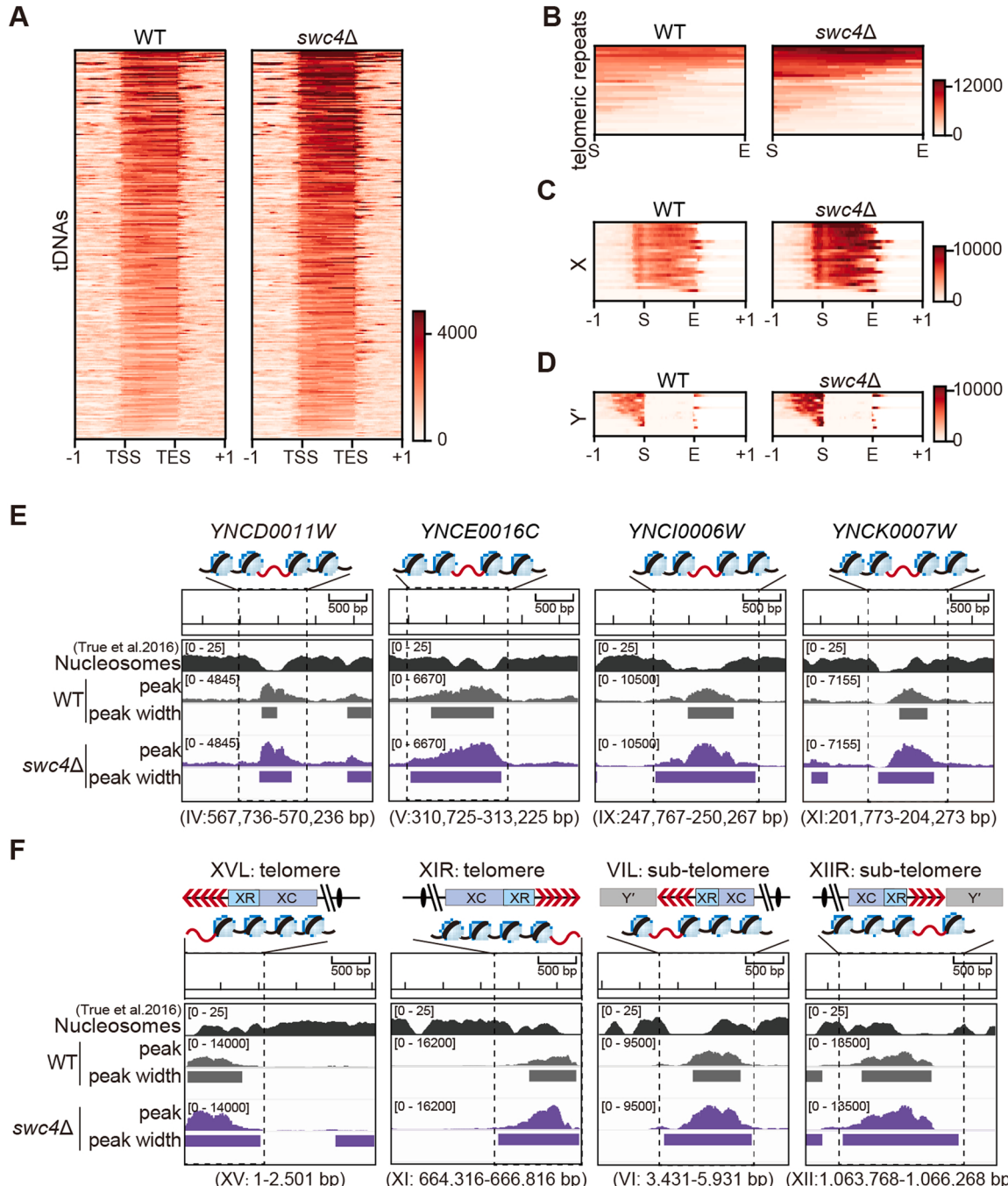


Fig. 6. Deletion of *SWC4* increases chromatin accessibility at tDNA and telomere regions. (A-D) Heatmaps of the enrichment of ATAC-seq peaks at all tDNA (A) and telomere regions (B-D) in wild-type and *swc4Δ* cells. (E) IGV browser shots comparison of nucleosome array, peak height and width at four specific tDNA regions. ATAC-seq peak files (BigWig format) were generated via bamCoverage version 1.5.11. The ATAC-seq peak width files were annotated with the software HMMRATAC version 1.2.10. (F) IGV browser shots comparison of nucleosome array, peak height and width at four specific telomere regions.

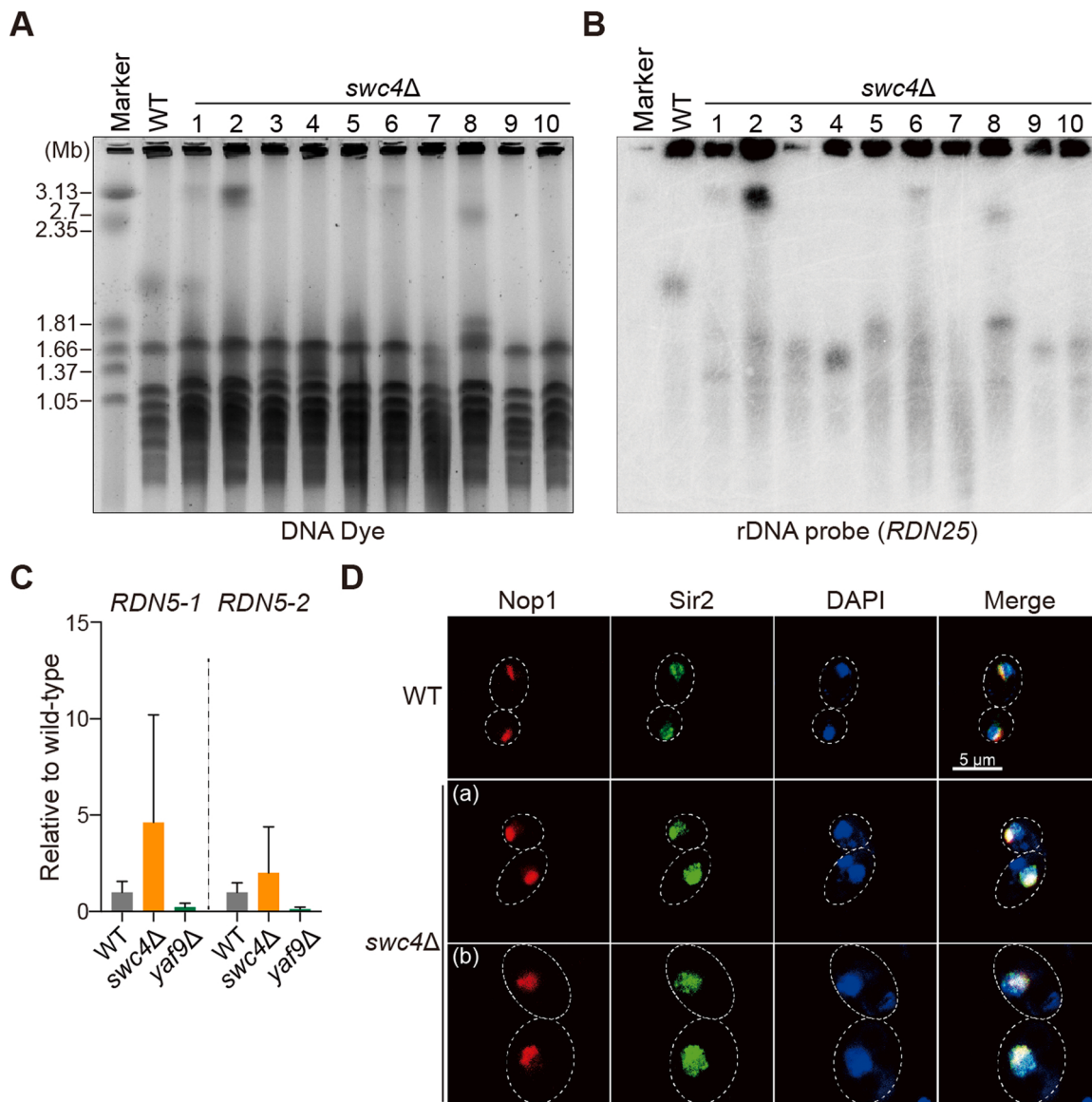


Fig. 7. Genome instability analyses at rDNA loci in *swc4Δ* cells. (A) Karyotype analysis of wild-type and *swc4Δ* strains. The chromosomes were separated by pulsed field gel electrophoresis (PFGE). The PFGE marker is indicated on the left of the panel. (B) Southern blotting analysis of the Chr XII in wild-type and *swc4Δ* strains. The *RDN25* gene (encoding 25 S rRNA, located on Chr XII) was labeled to probe Chr XII. (C) Enrichment of γ-H2A at *RDN5-1* and *RDN5-2* regions. The anti-γ-H2A antibody was used to perform ChIP analysis. Data are means ± SD. (n = 3). (D) Nucleolar staining of *swc4Δ* cells. Nop1 (red), 13Myc-tagged Sir2 (green) and DNA (blue) were examined by immunofluorescence. Cell shape is depicted by dotted line.

the *swc4Δ* cells, the size of Chr XII was all different: larger in the clones of 1, 2, 6 and 8, but smaller in other clones examined (Fig. 7A and 7B), indicating the contraction or expansion of rDNA loci. Consistently, in *swc4Δ* cells, the level of γ-H2A at *RDN5-1* and *RDN5-2* was higher than that in wild-type cells (Fig. 7C); deletion of *YAF9* slightly reduced the association of γ-H2A at these two sites.

We also examined the structure of the nucleolus, where the rDNA is located, by immunostaining the nucleolar marker Nop1, as well as 13Myc-tagged Sir2. In wild-type cells, the nucleolus showed a crescent-shaped structure (Fig. 7D), whereas in *swc4Δ* cells, the nucleolus showed greatly enhanced and/or widely expanded Nop1 staining (Fig. 7D). Accordingly, the Sir2 signals were increased in the *swc4Δ* cells compared to the wild-type cells (Fig. 7D). One explanation is that the rDNA loci in *swc4Δ* cells are very unstable and may have undergone high frequency homologous recombination. The other explanation is that the increased rDNA signal in *swc4Δ* cells is due to the increased chromosome ploidy. These results support the notion that the rDNA loci become unstable,

and might have undergone rearrangement.

3.6. Homologous recombination of tDNAs and telomeres is increased in *swc4Δ* cells

Swc4 was enriched in the gene bodies of tDNAs (Fig. 4A). In the *swc4Δ* cells, tDNA regions became more accessible (Fig. 6A). To test whether the loss of *Swc4* affects the stability of tDNAs, we constructed several heterozygous diploid strains, each containing a *URA3* marker flanked by identical tRNA^{Leu} genes (*SUP53-URA3-SUP53*, *SUS* in Fig. 8A and 8B) in one of Chr III. The isogenic haploid wild-type (WT^{SUS}), *swc4Δ*^{SUS} and the *yaf9Δ*^{SUS} strains were obtained through tetrad dissection after sporulation. Homologous recombination mediated loss of *URA3* marker was calculated on 5'-FOA plates [64]. The WT^{SUS} cells showed a 5'-FOA resistance rate of about 1.2×10^{-5} on median (Fig. 8B). In contrast, the *swc4Δ*^{SUS} cells showed a resistance rate of about 3.3×10^{-4} , ~28-fold higher than that of the WT^{SUS}. These results

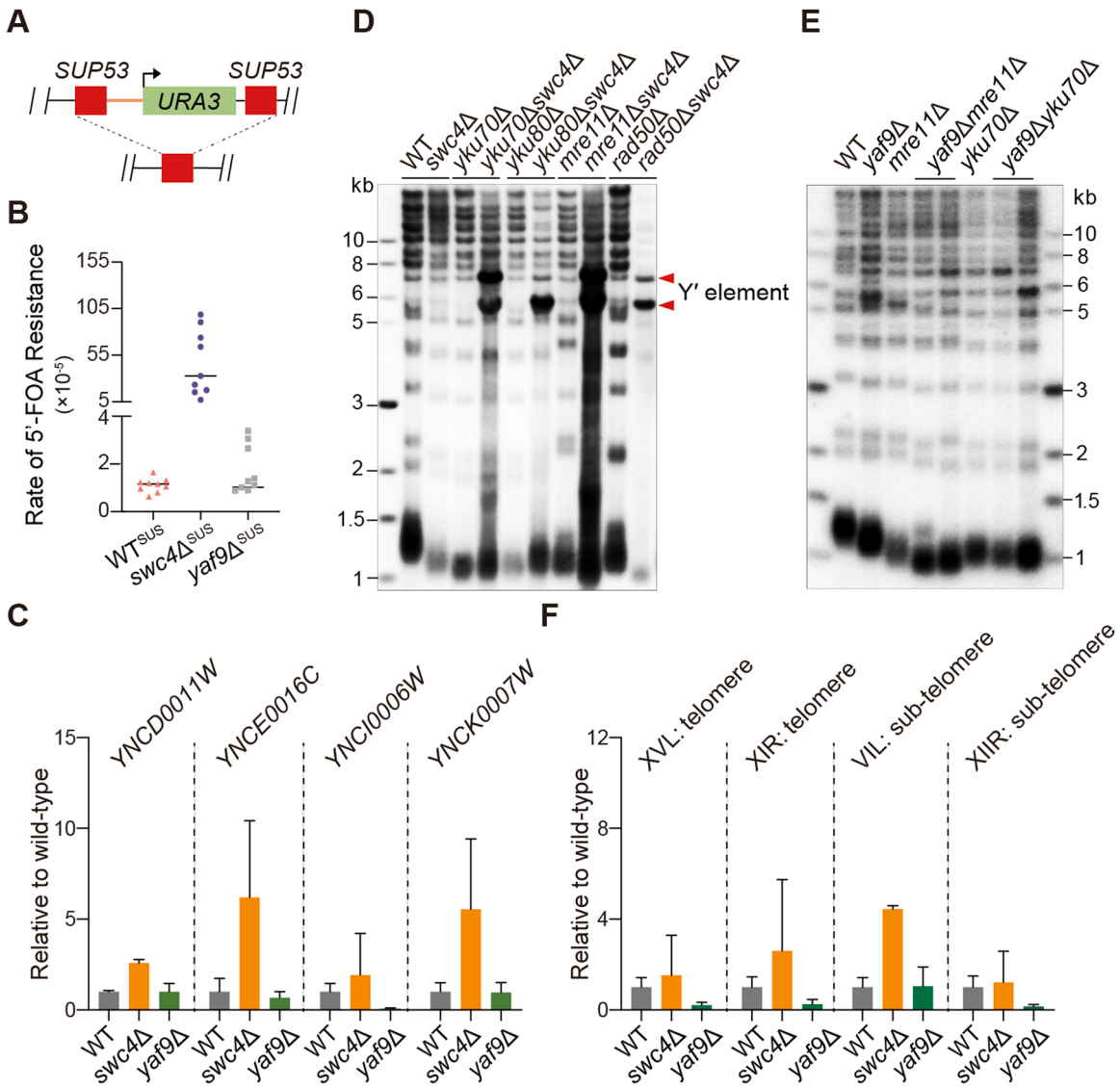


Fig. 8. Genome instability analyses at *SUP53s* and telomeres in *swc4Δ* cells. (A) Schematic diagram of homologous recombination between the two tandem *SUP53* tRNA^{Leu} genes. (B) Rates of 5'-FOA resistance in WT^{SUS}, *swc4Δ^{SUS}* and *yaf9Δ^{SUS}* cells. The rates were assayed with the system described in materials and methods. (C) Enrichment of γ-H2A at four tDNA regions. The anti-γ-H2A antibody was used to perform ChIP analysis. Data are means ± SD (n = 3). (D and E) Southern blotting analysis of telomere structure in the indicated strains labeled on top. The telomeric Y' elements are indicated by red arrowheads. (F) Enrichment of γ-H2A at four telomere regions. The anti-γ-H2A antibody was used to perform ChIP analysis. Data are means ± SD. (n = 3).

indicated that the tDNAs in the *swc4Δ* cells were much more susceptible to damage than in the wild-type cells. The genome instability in the *swc4Δ* cells could also be reflected by the wide range of marker loss rates from 7.1×10^{-5} to 9.9×10^{-4} (Fig. 8B). The *yaf9Δ^{SUS}* cells showed a 5'-FOA resistance rate of about 1.0×10^{-5} on median, which was slightly lower than that in wild-type cells (1.2×10^{-5}) (Fig. 8B). This result is consistent with the ChIP-seq data that more Swc4 was detected in the tRNA genes (Fig. 3B, Figs. S7A and 7B) in the absence of Yaf9 (Fig. 8B). In addition, the enrichment of γ-H2A at four tDNA loci (YNCD0011W, YNCE0016C, YNCI0006W and YNCK0007W) was significantly increased upon *SWC4* deletion (Fig. 8C).

Telomeric regions at chromosome ends contain the X elements, Y' elements and TG₁₋₃/C₁₋₃A repetitive sequences, which are hotspots for HR upon telomere deprotection [15,21]. We constructed diploid strains, which are heterozygous for *SWC4* and *YKU70* (or *YKU80*). The single and double deletion mutants were obtained through tetrad dissection after sporulation. All the double mutant spores of *swc4Δ yku70Δ* and *swc4Δ yku80Δ* showed severe growth defects immediately after germination (Fig S10). Further Southern blotting results revealed significant

telomere recombination, i.e. Y' element amplification occurred to repair telomeres in these mutants (Fig. 8D). Correspondingly, Y' element amplification and synthetic growth defects were also observed in the *swc4Δ mre11Δ* and *swc4Δ rad50Δ* double mutants (Fig. 8D and Fig S10). In contrast, the *yaf9Δ yku70Δ* and *yaf9Δ mre11Δ* did not double mutants showed no synthetic growth defect or telomere recombination (Fig. 8E and Fig S11). These results were consistent with the fact that Swc4 associates with telomeric regions in both wild-type and *yaf9Δ* cells (Fig. 4A and B), further supporting that the role of Swc4 at telomeres is independent of Yaf9. The level of γ-H2A at four specific telomeric/subtelomeric regions (i.e. the telomeric regions of Tel XVL and Tel XIR) was increased in the *swc4Δ* cells (Fig. 8F). Since both Yku and the MRX (Mre11-Rad50-Xrs2) complex are indispensable for telomere protection [17,41,82], we concluded that Swc4 plays a role in telomere protection, and that the protective role of Swc4 at telomeres is independent of Yku and MRX as well. These results also provide a plausible explanation for our previous observation that deletion of *SWC4* accelerates the senescence of telomerase-deficient cells [44].

3.7. Arp4 associates with RDN5s, tDNAs and telomeres

Arp4 physically interacts with Swc4 [66]. Temperature sensitive *arp4* mutants grown at restrictive temperatures show abnormalities in cell shape, bulk chromatin organization and formation of the chromosome segregation apparatus [19,57], similar to those observed in *swc4Δ* cells (Fig. 1). Biochemical analysis has shown that C-terminus of Arp4 binds linker DNA and functions as a DNA-length sensor that regulates nucleosome sliding [10]. Recent structural data suggest that the lysine patch of Swc4 (including Lys311, Lys314 and Lys316) may interact with DNA [66]. We proposed that Arp4 also associates with the NFRs of chromatin to recruit Swc4. To test this, we performed ChIP-seq analysis with 3Flag-tagged Arp4 cells, and identified 1432 ChIP-seq peaks of Arp4 (Fig S12). Further analysis revealed that that 73% of the Swc4 ChIP-seq peaks overlapped with 33% of the Arp4 ChIP-seq peaks (Fig S12). In addition, the enrichment of Arp4 at all *RDN5s*, tDNAs and telomere regions was significant (Fig. 9A-F), suggesting that like Swc4, Arp4 associates with NFRs. These results consistently support the

conclusion that Swc4 protects NFRs to inhibit genome instability.

4. Discussion

Previous studies suggested that NuA4 and SWR1-C share the Act1-Arp4-Swc4-Yaf9 submodule, which plays a recruitment role in histone acetylation and H2A.Z deposition, respectively [47]. However, inactivation of Swc4 or Yaf9 does not abolish histone acetylation or H2A.Z chromatin incorporation [3,44,87]. In addition, deletion of *EAF1* disassembles the NuA4 complex [3], and deletion of *SWR1* affects the assembly of SWR1-C [84]. However, the *yaf9Δ*, *swr1Δ* and *eaf1Δ* mutant cells grow as robustly as wild-type cells (Fig. 1A and Fig S1A). Consistently, the phenotypes of aneuploidy and genome instability in *swc4Δ* cells are not observed in *yaf9Δ* cells (Figs. 1-2 and Fig S1-S4), but rather resemble the defects detected in the *arp4* temperature sensitive mutant [19,57]. Together, these findings suggest that the essentiality of Swc4 or Arp4, in chromatin is not the recruitment of either NuA4 or SWR1-C onto chromatin.

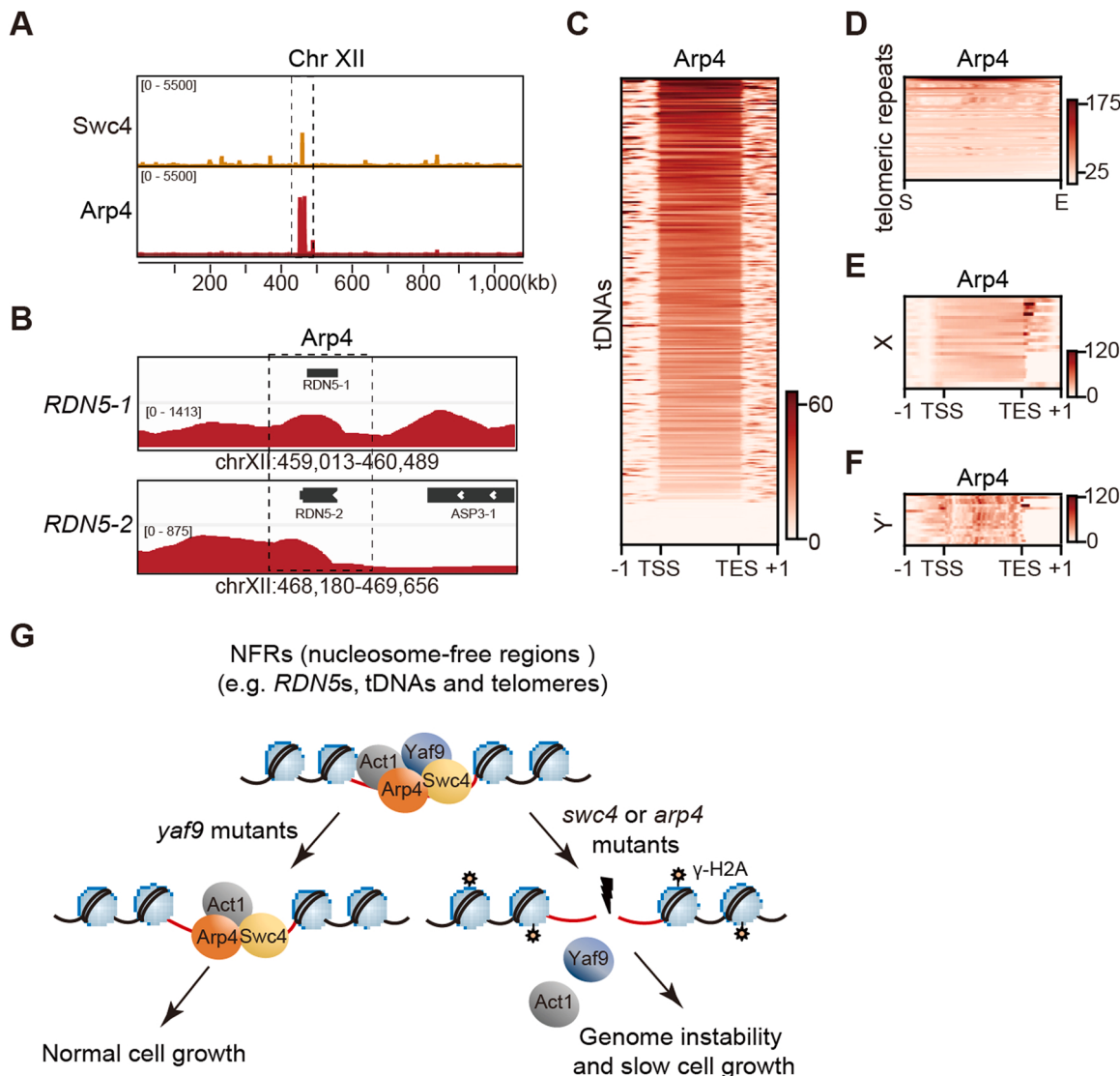


Fig. 9. (A) IGV browser shot comparison of ChIP-seq (13Myc-tagged Swc4 and 3Flag-tagged Arp4) signals at Chr XII in wild-type cells. (B) IGV browser shot comparison of ChIP-seq signals of 3Flag-tagged Arp4 at *RDN5-1* and *RDN5-2* in wild-type cells. (C-F) Heatmaps of the enrichment of 3Flag-tagged Arp4 at all tDNA (C) and telomere (D-F) regions in wild-type cells. (G) A working model of Swc4 in chromatin protection. In wild-type cells, Swc4 forms a complex with Arp4, Yaf9 and Act1, binds NFRs of chromatin, Arp4 binds linker DNA (Brahma et al., 2018), and Swc4 cooperates with Arp4 to protect the fragile chromatin to inhibit genome instability. In the absence of Yaf9 (*yaf9Δ*), Swc4 (as well as Arp4) still associates with and protects chromatin, the cell proliferation remains unchanged. In the absence of Swc4 or Arp4 (*swc4Δ* and/or *arp4* mutants), chromosomes are prone to break and the γ-H2A level is increased, and the genome becomes unstable.

Swc4 associates with chromatin at numerous sites (Fig. 3B and Supplementary Table S2), including the *RND5* genes in rDNA loci, tDNAs and telomeres, which are representative of NFRs [60,69]. Both the *RDN5*s and tDNAs are transcribed by RNA Pol III. It is unclear what the determinants are for Swc4 targeting to these loci. One possibility is that the DNA sequences in these loci contain common features that remain to be elucidated. Another possibility is that there may be unidentified secondary structure at the DNA level. A third possibility is that Arp4 recruits Swc4 to the NFRs, given that Arp4 binds linker DNA [10], and associates with NFRs *in vivo* (Fig. 9A-9F) [69].

Nucleosomes have evolved to facilitate the packaging of genomic DNA, and to regulate chromatin activities such as replication, gene expression and silencing. A significant proportion of the eukaryotic genome is nucleosome-free. For example, there are over 14,000 NFRs in the yeast genome [27]. NFRs are associated with, and likely protected by, different types of proteins and protein complexes. In the case of the Act1-Arp4-Swc4-Yaf9 complex, both Arp4 and Swc4 associate with NFRs such as telomere regions and tDNAs (Figs. 3, 4 and 9A-9F) [57,69]. The phenotypes observed in the *arp4-ts* mutants, such as larger cell size (as well as larger nuclei) [19,77], abnormal chromatin structure [23], and chromosome breakage [12], are also seen in the *swc4Δ* cells (Fig. 1, Fig. S1-S4). In contrast, the *yaf9Δ* mutant has few defects in genome stability or cell growth (Fig. 1 and Fig S1-S4), suggesting that Yaf9 is less indispensable than either Arp4 or Swc4 in chromatin activities. Although both Arp4 and Swc4 are considered to be the components of NuA4 and SWR1-C, disassembly of either NuA4 or SWR1-C does not cause the growth defects seen in either the *swc4Δ* cells (Fig. 1A and Fig. S1A) or the *arp4-ts* mutants [57]. The association of Swc4 with the nucleosome-free chromatin of rDNA, tDNA and telomere loci is independent of Yaf9, Eaf1 or Swr1 (Figs. 3–4 and Fig S5-S9). Furthermore, the absence of Swc4, but not Yaf9, increases the accessibility and fragility of NFRs (Figs. 5–6). Thus, the primary role of Swc4 and Arp4 in chromatin is likely to protect the fragile NFRs of rDNAs, tDNAs and telomeres to ensure genome stability (Fig. 9G). In the absence of Swc4 (or Arp4), the NFRs of rDNAs, tDNAs and telomeres become more vulnerable to various damages, leading to chromosome breaks and poor cell viability (Fig. 9G).

Author contribution

J.Q.Z., J.C.L. and Y.P. conceived and designed the experiments; Y.P., J.C.L., C.h. and Lin-Jun Hou (bioinformatics analysis for ATAC-seq data), Yu-Long Chen (bioinformatics analysis for ChIP-seq data) performed the experiments; J.Q.Z. and J.C.L. wrote the paper with input from all co-authors; J.Q.Z., J.C.L. and Jiantao Shi supervised the study.

Funding

This work was supported by grants from the National Key Research and Development Program of China [2019YFA0109902]; Shanghai Research Project [18JC1420202].

CRediT authorship contribution statement

Yue Pan: Methodology, Validation, Investigation, Visualization, Writing - Original Draft. **Can Hu:** Validation, Investigation, Visualization. **Lin-Jun Hou:** Software, Formal analysis, Visualization. **Yu-Long Chen:** Software, Formal analysis, Visualization. **Jiantao Shi:** Software, Project administration and Supervision. **Jia-Cheng Liu:** Conceptualization, Methodology, Investigation, data curation, Writing - Original Draft. **Jin-Qiu Zhou:** Conceptualization, Resources, Writing - Review & Editing, Supervision, and Funding acquisition.

Declaration of Competing Interest

The authors declare that there are no conflicts of interest.

Data availability

The ChIP-seq data and ATAC-seq data of this study have been submitted to GEO (Gene Expression Omnibus) of NCBI under accession number GSE215374 and GSE202946, respectively.

Acknowledgement

We thank the members of the Zhou lab for the help, discussions and suggestions. The ChIP-seq data and ATAC-seq data of this study have been submitted to GEO (Gene Expression Omnibus) of NCBI under accession numbers GSE215374 and GSE202946, respectively. GSE215374 (ChIP-seq) and GSE202946 (ATAC-seq) have been unified under GSE215375 (<https://www.ncbi.nlm.nih.gov/geo/query/acc.cgi?acc=GSE215375>).

Appendix A. Supporting information

Supplementary data associated with this article can be found in the online version at doi:[10.1016/j.dnarep.2023.103512](https://doi.org/10.1016/j.dnarep.2023.103512).

References

- [1] A. Adey, H.G. Morrison, Asan, X. Xun, J.O. Kitzman, E.H. Turner, B. Stackhouse, A. P. MacKenzie, N.C. Caruccio, X. Zhang, et al., Rapid low-input low-bias construction of shotgun fragment libraries by high-density in vitro transposition, *Genome Biol.* 11 (2010) R119.
- [2] S. Allard, R.T. Utley, J. Savard, A. Clarke, P. Grant, C.J. Brandl, L. Pillus, J. L. Workman, J. Cote, NuA4, an essential transcription adaptor/histone H4 acetyltransferase complex containing Esa1p and the ATM-related cofactor Tra1p, *EMBO J.* 18 (1999) 5108–5119.
- [3] A. Auger, L. Galarneau, M. Altaf, A. Nourani, Y. Doyon, R.T. Utley, D. Cronier, S. Allard, J. Cote, Eaf1 is the platform for NuA4 molecular assembly that evolutionarily links chromatin acetylation to ATP-dependent exchange of histone H2A variants, *Mol. Cell Biol.* 28 (2008) 2257–2270.
- [4] P.B. Becker, J.L. Workman, Nucleosome remodeling and epigenetics, *Cold Spring Harb. Perspect. Biol.* 5 (2013).
- [5] J.A. Belsky, H.K. MacAlpine, Y. Lubelsky, A.J. Hartemink, D.M. MacAlpine, Genome-wide chromatin footprinting reveals changes in replication origin architecture induced by pre-RC assembly, *Genes Dev.* 29 (2015) 212–224.
- [6] G.A. Bentley, A. Lewitbentley, J.T. Finch, A.D. Podjarny, M. Roth, Crystal-structure of the nucleosome core particle at 16 Å resolution, *J. Mol. Biol.* 176 (1984) 55–75.
- [7] C.B. Bittner, D.T. Zeisig, B.B. Zeisig, R.K. Slany, Direct physical and functional interaction of the NuA4 complex components Yaf9p and Swc4p, *Eukaryot. Cell* 3 (2004) 976–983.
- [8] A.A. Boudreault, D. Cronier, W. Selleck, N. Lacoste, R.T. Utley, S. Allard, J. Savard, W.S. Lane, S. Tan, J. Cote, Yeast enhancer of polycomb defines global Esa1-dependent acetylation of chromatin, *Genes Dev.* 17 (2003) 1415–1428.
- [9] A.P. Boyle, S. Davis, H.P. Shulha, P. Meltzer, E.H. Margulies, Z. Weng, T.S. Furey, G.E. Crawford, High-resolution mapping and characterization of open chromatin across the genome, *Cell* 132 (2008) 311–322.
- [10] S. Brahma, M. Ngubo, S. Paul, M. Udagama, B. Bartholomew, The Arp8 and Arp4 module acts as a DNA sensor controlling INO80 chromatin remodeling, *Nat. Commun.* 9 (2018) 3309.
- [11] J.D. Buenrostro, P.G. Giresi, L.C. Zaba, H.Y. Chang, W.J. Greenleaf, Transposition of native chromatin for fast and sensitive epigenomic profiling of open chromatin DNA-binding proteins and nucleosome position, *Nat. Methods* 10 (2013) 1213–1218.
- [12] E. Cheng, J.A. Vaisica, J. Ou, A. Baryshnikova, Y. Lu, F.P. Roth, G.W. Brown, Genome rearrangements caused by depletion of essential DNA replication proteins in *Saccharomyces cerevisiae*, *Genetics* 192 (2012) 147–160.
- [13] A.S. Clarke, J.E. Lowell, S.J. Jacobson, L. Pillus, Esa1p is an essential histone Acetyltransferase required for cell cycle progression, *Mol. Cell. Biol.* 19 (1999) 2515–2526.
- [14] J.A. Downs, N.F. Lowndes, S.P. Jackson, A role for *Saccharomyces cerevisiae* histone H2A in DNA repair, *Nature* 408 (2000) 1001–1004.
- [15] M.L. DuBois, Z.W. Haimberger, M.W. McIntosh, D.E. Gottschling, A quantitative assay for telomere protection in *Saccharomyces cerevisiae*, *Genetics* 161 (2002) 995–1013.
- [16] S.J. Elledge, Cell cycle checkpoints: preventing an identity crisis, *Science* 274 (1996) 1664–1672.
- [17] S.S. Foster, M.K. Zubko, S. Guillard, D. Lydall, MRX protects telomeric DNA at uncapped telomeres of budding yeast cdc13-1 mutants, *DNA Repair* 5 (2006) 840–851.
- [18] G. Fourel, E. Revardel, C.E. Koering, E. Gilson, Cohabitation of insulators and silencing elements in yeast subtelomeric regions, *EMBO J.* 18 (1999) 2522–2537.
- [19] M. Georgieva, M. Harata, G. Miloshev, The nuclear actin-related protein Act3p/Arp4 influences yeast cell shape and bulk chromatin organization, *J. Cell Biochem.* 104 (2008) 59–67.

- [20] G. Giaever, A.M. Chu, L. Ni, C. Connelly, L. Riles, S. Veronneau, S. Dow, A. Lucau-Danila, K. Anderson, B. Andre, et al., Functional profiling of the *Saccharomyces cerevisiae* genome, *Nature* 418 (2002) 387–391.
- [21] N. Grandin, M. Charbonneau, The rad51 pathway of telomerase-independent maintenance of telomeres can amplify TG(1-3) sequences in yku and cdc13 mutants of *Saccharomyces cerevisiae*, *Mol. Cell. Biol.* 23 (2003) 3721–3734.
- [22] J. Gutin, R. Sadeh, N. Bodenheimer, D. Joseph-Strauss, A. Klein-Brill, A. Alajem, O. Ram, N. Friedman, Fine-resolution mapping of TF binding and chromatin interactions, *Cell Rep.* 22 (2018) 2797–2807.
- [23] M. Harata, Y. Oma, S. Mizuno, Y.W. Jiang, D.J. Stillman, U. Wintersberger, The nuclear actin-related protein of *Saccharomyces cerevisiae* Act3p/Arp4, interacts with core histones, *Mol. Biol. Cell* 10 (1999) 2595–2605.
- [24] K.G. Hardwick, A.W. Murray, Mad1p, a phosphoprotein component of the spindle assembly checkpoint in budding yeast, *J. Cell Biol.* 131 (1995) 709–720.
- [25] M.H. He, J.C. Liu, Y.S. Lu, Z.J. Wu, Y.Y. Liu, Z. Wu, J. Peng, J.Q. Zhou, KEOPS complex promotes homologous recombination via DNA resection, *Nucleic Acids Res.* (2019).
- [26] Y. Ichikawa, N. Morohashi, Y. Nishimura, H. Kurumizaka, M. Shimizu, Telomeric repeats act as nucleosome-disfavouring sequences in vivo, *Nucleic Acids Res.* 42 (2014) 1541–1552.
- [27] C. Jiang, B.F. Pugh, A compiled and systematic reference map of nucleosome positions across the *Saccharomyces cerevisiae* genome, *Genome Biol.* 10 (2009) R109.
- [28] C. Jiang, B.F. Pugh, Nucleosome positioning and gene regulation: advances through genomics, *Nat. Rev. Genet.* 10 (2009) 161–172.
- [29] E. Kassabini, D.E. Pefani, S. Taraviras, Z. Lygerou, Ribosomal DNA and the nucleolus at the heart of aging, *Trends Biochem. Sci.* 47 (2022) 328–341.
- [30] M.C. Keogh, T.A. Mennella, C. Sawa, S. Berthelet, N.J. Krogan, A. Wolek, V. Podolny, L.R. Carpenter, J.F. Greenblatt, K. Baetz, et al., The *Saccharomyces cerevisiae* histone H2A variant Htz1 is acetylated by NuA4, *Gene Dev.* 20 (2006) 660–665.
- [31] D.A. Keys, B.S. Lee, J.A. Dodd, T.T. Nguyen, L. Vu, E. Fantino, L.M. Burson, Y. Nogi, M. Nomura, Multiprotein transcription factor UAF interacts with the upstream element of the yeast RNA polymerase I promoter and forms a stable preinitiation complex, *Gene Dev.* 10 (1996) 887–903.
- [32] A. Klein-Brill, D. Joseph-Strauss, A. Appleboim, N. Friedman, Dynamics of chromatin and transcription during transient depletion of the RSC chromatin remodeling complex, *Cell Rep.* 26 (2019) 279–292, e275.
- [33] B.J. Klein, S. Ahmad, K.R. Vann, F.H. Andrews, Z.A. Mayo, G. Bourriquet, J. Bridgers, J.Y. Zhang, B.D. Strahl, J. Cote, et al., Yaf9 subunit of the NuA4 and SWR1 complexes targets histone H3K27ac through its YEATS domain, *Nucleic Acids Res.* 46 (2018) 421–430.
- [34] M.S. Kobor, S. Venkatasubrahmanyam, M.D. Meneghini, J.W. Gin, J.L. Jennings, A. J. Link, H.D. Madhani, J. Rine, A protein complex containing the conserved Swi2/Snf2-related ATPase Swr1p deposits histone variant H2A.Z into euchromatin, *PLoS Biol.* 2 (2004), E131.
- [35] P. Konig, R. Giraldo, L. Chapman, D. Rhodes, The crystal structure of the DNA-binding domain of yeast RAP1 in complex with telomeric DNA, *Cell* 85 (1996) 125–136.
- [36] R.D. Kornberg, J.O. Thomas, Chromatin Structure: oligomers of the histones, *Science* 184 (1974) 865–868.
- [37] N. Krietenstein, M. Wal, S. Watanabe, B. Park, C.L. Peterson, B.F. Pugh, P. Korber, Genomic nucleosome organization reconstituted with pure proteins, *Cell* 167 (709–721) (2016), e712.
- [38] N.J. Krogan, M.C. Keogh, N. Datta, C. Sawa, O.W. Ryan, H.M. Ding, R.A. Haw, J. Pootoolal, A. Tong, V. Canadien, et al., A Snf2 family ATPase complex required for recruitment of the histone H2A variant Htz1, *Mol. Cell* 12 (2003) 1565–1576.
- [39] Y. Kumar, P. Bhargava, A unique nucleosome arrangement maintained actively by chromatin remodelers facilitates transcription of yeast tRNA genes, *BMC Genom.* 14 (2013) 402.
- [40] M.C. Lanz, D. Dibitetto, M.B. Smolka, DNA damage kinase signaling: checkpoint and repair at 30 years, *EMBO J.* 38 (2019), e101801.
- [41] M. Larrivee, C. LeBel, R.J. Wellinger, The generation of proper constitutive G-tails on yeast telomeres is dependent on the MRX complex, *Genes Dev.* 18 (2004) 1391–1396.
- [42] I. Le Masson, D.Y. Yu, K. Jensen, A. Chevalier, R. Courbeyrette, Y. Boulard, M. M. Smith, C. Mann, Yaf9, a novel NuA4 histone acetyltransferase subunit, is required for the cellular response to spindle stress in yeast, *Mol. Cell Biol.* 23 (2003) 6086–6102.
- [43] W. Lee, D. Tillo, N. Bray, R.H. Morse, R.W. Davis, T.R. Hughes, C. Nislow, A high-resolution atlas of nucleosome occupancy in yeast, *Nat. Genet.* 39 (2007) 1235–1244.
- [44] J.C. Liu, Q.J. Li, M.H. He, C. Hu, P. Dai, F.L. Meng, B.O. Zhou, J.Q. Zhou, Swc4 positively regulates telomere length independently of its roles in NuA4 and SWR1 complexes, *Nucleic Acids Res.* 48 (2020) 12792–12803.
- [45] M.S. Longtine, A. McKenzie, D.J. Demarini, N.G. Shah, A. Wach, A. Brachet, P. Philipsen, J.R. Pringle, Additional modules for versatile and economical PCR-based gene deletion and modification in *Saccharomyces cerevisiae*, *Yeast* 14 (1998) 953–961.
- [46] Y. Lorch, B. Maier-Davis, R.D. Kornberg, Role of DNA sequence in chromatin remodeling and the formation of nucleosome-free regions, *Genes Dev.* 28 (2014) 2492–2497.
- [47] P.Y. Lu, N. Levesque, M.S. Kobor, NuA4 and SWR1-C: two chromatin-modifying complexes with overlapping functions and components, *Biochem. Cell Biol.* 87 (2009) 799–815.
- [48] K. Luger, A.W. Mäder, R.K. Richmond, D.F. Sargent, T.J. Richmond, Crystal structure of the nucleosome core particle at 2.8 Å resolution, *Nature* 389 (1997) 251–260.
- [49] R.J. McFarlane, S.K. Whitehall, tRNA genes in eukaryotic genome organization and reorganization, *Cell Cycle* 8 (2009) 3102–3106.
- [50] F.L. Meng, Y. Hu, N. Shen, X.J. Tong, J. Wang, J. Ding, J.Q. Zhou, Sua5p a single-stranded telomeric DNA-binding protein facilitates telomere replication, *EMBO J.* 28 (2009) 1466–1478.
- [51] A. Miciakiewicz, A. Chelstowska, The essential function of Swc4p - a protein shared by two chromatin-modifying complexes of the yeast *Saccharomyces cerevisiae* - resides within its N-terminal part, *Acta Biochim. Pol.* 55 (2008) 603–612.
- [52] C.B. Millar, M. Grunstein, Genome-wide patterns of histone modifications in yeast, *Nat. Rev. Mol. Cell Bio.* 7 (2006) 657–666.
- [53] L. Mitchell, J.P. Lambert, M. Gerdes, A.S. Al-Madhoun, I.S. Skerjanc, D. Figgeys, K. Baetz, Functional dissection of the NuA4 histone acetyltransferase reveals its role as a genetic hub and that Eaf1 is essential for complex integrity, *Mol. Cell Biol.* 28 (2008) 2244–2256.
- [54] M. Mivelaz, A.M. Cao, S. Kubik, S. Zencir, R. Hovius, I. Boichenko, A. M. Stachowicz, C.F. Kurat, D. Shore, B. Fierz, Chromatin fiber invasion and nucleosome displacement by the Rap1 transcription factor, *Mol. Cell* 77 (2020) 488–500, e489.
- [55] G. Mizuguchi, X.T. Shen, J. Landry, W.H. Wu, S. Sen, C. Wu, ATP-Driven exchange of histone H2A2 variant catalyzed by SWR1 chromatin remodeling complex, *Science* 303 (2004) 343–348.
- [56] E. Oberbeckmann, M. Wolff, N. Krietenstein, M. Heron, J.L. Ellins, A. Schmid, S. Krebs, H. Blum, U. Gerland, P. Korber, Absolute nucleosome occupancy map for the *Saccharomyces cerevisiae* genome, *Genome Res.* 29 (2019) 1996–2009.
- [57] H. Ogiwara, A. Ui, S. Kawashima, K. Kugou, F. Onoda, H. Iwashashi, M. Harata, K. Ohta, T. Enomoto, M. Seki, Actin-related protein Arp4 functions in kinetochore assembly, *Nucleic Acids Res.* 35 (2007) 3109–3117.
- [58] P. Oudet, M. Grossbellard, P. Chambon, Electron-microscopic and biochemical evidence that chromatin structure is a repeating unit, *Cell* 4 (1975) 281–300.
- [59] E.A. Ozonov, E. van Nimwegen, Nucleosome free regions in yeast promoters result from competitive binding of transcription factors that interact with chromatin modifiers, *Plos Comput. Biol.* 9 (2013).
- [60] A. Panday, A. Grove, Yeast HMO1: linker histone reinvented, *Microbiol. Mol. Biol. Rev.* 81 (2017).
- [61] E. Pasquier, R.J. Wellinger, In vivo chromatin organization on native yeast telomeric regions is independent of a cis-telomere loopback conformation, *Epigenet. Chromatin* 13 (2020).
- [62] J. Peng, J.Q. Zhou, The tail-module of yeast Mediator complex is required for telomere heterochromatin maintenance, *Nucleic Acids Res.* 40 (2012) 581–593.
- [63] O. Pericic, R. Collepardo-Guevara, T. Schlick, Modeling studies of chromatin fiber structure as a function of DNA linker length, *J. Mol. Biol.* 403 (2010) 777–802.
- [64] M.J. Pratt-Hyatt, K.M. Kapadia, T.E. Wilson, D.R. Engelke, Increased recombination between active rRNA genes, *DNA Cell Biol.* 25 (2006) 359–364.
- [65] M. Preti, C. Ribeyre, C. Pascali, M.C. Bosio, B. Cortelazzi, J. Rougemont, E. Guarnera, F. Naeff, D. Shore, G. Dieci, The telomere-binding protein Tbf1 demarcates snoRNA gene promoters in *Saccharomyces cerevisiae*, *Mol. Cell* 38 (2010) 614–620.
- [66] K. Qu, K. Chen, H. Wang, X. Li, Z. Chen, Structure of the NuA4 acetyltransferase complex bound to the nucleosome, *Nature* (2022).
- [67] O.J. Rando, F. Winston, Chromatin and transcription in yeast, *Genetics* 190 (2012) 351–387.
- [68] A. Ranjan, G. Mizuguchi, P.C. Fitzgerald, D. Wei, F. Wang, Y. Huang, E. Luk, C. L. Woodcock, C. Wu, Nucleosome-free region dominates histone acetylation in targeting SWR1 to promoters for H2A.Z replacement, *Cell* 154 (2013) 1232–1245.
- [69] M.J. Rossi, P.K. Kuntala, W.K.M. Lai, N. Yamada, N. Badjatia, C. Mittal, G. Kuzu, K. Bocklund, N.P. Farrell, T.R. Blanda, et al., A high-resolution protein architecture of the budding yeast genome, *Nature* 592 (2021) 309–314.
- [70] W. Selleck, I. Fortin, D. Sermwittayawong, J. Cote, S. Tan, The *Saccharomyces cerevisiae* Piccolo NuA4 histone acetyltransferase complex requires the enhancer of polycomb a domain and chromodomain to acetylate nucleosomes, *Mol. Cell Biol.* 25 (2005) 5535–5542.
- [71] Y. Shao, N. Lu, Z. Wu, C. Cai, S. Wang, L.-L. Zhang, F. Zhou, S. Xiao, L. Liu, X. Zeng, et al., Creating a functional single-chromosome yeast, *Nature* (2018).
- [72] R.S. Sikorski, P. Hieter, A system of shuttle vectors and yeast host strains designed for efficient manipulation of DNA in *Saccharomyces-Cerevisiae*, *Genetics* 122 (1989) 19–27.
- [73] D.A. Sinclair, L. Guarente, Extrachromosomal rRNA circles-a cause of aging in yeast, *Cell* 91 (1997) 1033–1042.
- [74] V.K. Singh, A. Krishnamachari, Context based computational analysis and characterization of ARS consensus sequences (ACS) of *Saccharomyces cerevisiae* genome, *Genom. Data* 9 (2016) 130–136.
- [75] R.V. Skibbens, P. Hieter, Kinetochore and the checkpoint mechanism that monitors for defects in the chromosome segregation machinery, *Annu. Rev. Genet.* 32 (1998) 307–337.
- [76] J.S. Steffan, D.A. Keys, J.A. Dodd, M. Nomura, The role of TBP in rDNA transcription by RNA polymerase I in *Saccharomyces cerevisiae*: TBP is required for upstream activation factor-dependent recruitment of core factor, *Gene Dev.* 10 (1996) 2551–2563.
- [77] F. Steinbock, L. Krupanska, A. Bogusch, A. Kaufmann, E. Heidenreich, Novel regulatory properties of *Saccharomyces cerevisiae* Arp4, *J. Biochem.* 139 (2006) 741–751.

- [78] A. Stepanchick, H.J. Zhi, A.H. Cavanaugh, K. Rothblum, D.A. Schneider, L. I. Rothblum, DNA Binding by the ribosomal DNA Transcription Factor Rrn3 is essential for ribosomal DNA Transcription, *J. Biol. Chem.* 288 (2013) 9135–9144.
- [79] K. Struhl, E. Segal, Determinants of nucleosome positioning, *Nat. Struct. Mol. Biol.* 20 (2013) 267–273.
- [80] R.K. Szilard, P.E. Jacques, L. Laramee, B. Cheng, S. Galicia, A.R. Bataille, M. Yeung, M. Mendez, M. Bergeron, F. Robert, et al., Systematic identification of fragile sites via genome-wide location analysis of gamma-H2AX, *Nat. Struct. Mol. Biol.* 17 (2010) 299–305.
- [81] J.D. True, J.J. Muldoon, M.N. Carver, K. Poorey, S.J. Shetty, S. Bekiranov, D. T. Auble, The modifier of transcription 1 (Mot1) ATPase and Spt16 histone chaperone co-regulate transcription through preinitiation complex assembly and nucleosome organization, *J. Biol. Chem.* 291 (2016) 15307–15319.
- [82] Y. Tsukamoto, A.K.P. Taggart, V.A. Zakian, The role of the Mre11-Rad50-Xrs2 complex in telomerase-mediated lengthening of *Saccharomyces cerevisiae* telomeres, *Curr. Biol.* 11 (2001) 1328–1335.
- [83] J. Venema, D. Tollervey, Ribosome synthesis in *Saccharomyces cerevisiae*, *Annu. Rev. Genet.* 33 (1999) 261–311.
- [84] W.H. Wu, S. Alami, E. Luk, C.H. Wu, S. Sen, G. Mizuguchi, D. Wei, C. Wu, Swc2 is a widely conserved H2AZ-binding module essential for ATP-dependent histone exchange, *Nat. Struct. Mol. Biol.* 12 (2005) 1064–1071.
- [85] W.H. Wu, C.H. Wu, A. Ladurner, G. Mizuguchi, D. Wei, H. Xiao, E. Luk, A. Ranjan, C. Wu, N terminus of Swr1 binds to histone H2AZ and provides a platform for subunit assembly in the chromatin remodeling complex, *J. Biol. Chem.* 284 (2009) 6200–6207.
- [86] K.Y. Yen, V. Vinayachandran, B.F. Pugh, SWR-C and INO80 chromatin remodelers recognize nucleosome-free regions Near+1 nucleosomes, *Cell* 154 (2013) 1246–1256.
- [87] B.O. Zhou, S.S. Wang, L.X. Xu, F.L. Meng, Y.J. Xuan, Y.M. Duan, J.Y. Wang, H. Hu, X. Dong, J. Ding, et al., SWR1 complex poises heterochromatin boundaries for antisilencing activity propagation, *Mol. Cell Biol.* 30 (2010) 2391–2400.
- [88] J. Zhou, B.O. Zhou, B.A. Lenzmeier, J.Q. Zhou, Histone deacetylase Rpd3 antagonizes Sir2-dependent silent chromatin propagation, *Nucleic Acids Res.* 37 (2009) 3699–3713.